FRERES MENTOURI UNIVERSITY
CONSTANTINE 1 -ALGERIA

Journal of Sciences & Technology

Semestrial Journal of Freres Mentouri University, Constantine, Algeria

VOLUME 03 - ISSUE 01— JUNE 2018

EISSN: ….-….

Freres Mentouri
University Constantine

Ain El-Bey Road
Constantine 25000
Algeria

Phone.Fax: 213 (0) 31. 81. 12.78
Email: revues@umc.edu.dz
Website :http://revue.umc.edu.dz

Journal of Sciences & Technology

Volume 3 N° 1 - June 2018

Semestrial Journal of Freres Mentouri Constantine 1 University, Algeria

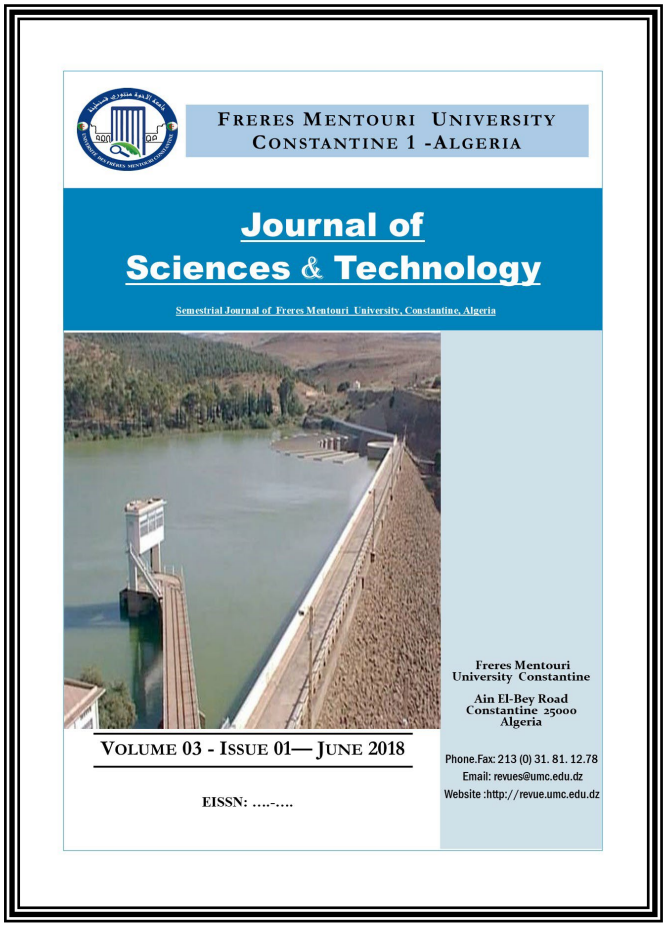

An article proposed for publication should not be submitted at the same time to another journal.

Manuscripts (original and two copies) should be sent to the following address:

Vice-Rectorate in charge of Post-Graduation and Scientific Research

Direction of Publications and Scientific Animation (15th floor)

Constantine 1 University , Aïn-El-Bey Road, 25000 Constantine, ALGERIA.

Tél./Fax: 213 (0) 31.81.12.78

e-mail: revues@umc.edu.dz

Constantine1 University

Journal of Sciences & Technology

Volume 3 N° 1 – June 2018

SCIENTIFIC COMMITTEE

INSTRUCTIONS TO AUTHORS

I- Overview

The journal Human Sciences publishes in three languages: Arabic, French and English. Two abstracts must be provided, one in the language of the article, the other in Arabic if the article is written in another language, or in French (or English) if the article is written in Arabic. Abstracts must not exceed 150 words. Unpublished articles are not returned to their authors.

II- Manuscrips

The articles submitted for publication (three copies) must not exceed 20 typewritten pages (tables, figures, graphs, bibliography, ... included) with a large margin to the left (3 cm), printed on 21 x 29 paper , 7 cm (A4) with interligne of good readability. Some flexibility is allowed to authors, but they should organize the text clearly in sections such as: Introduction, Experimental Details, Results, Discussion and Conclusion. The longer articles will be published by part in successive issues, each part being determined by the authors. Authors are kindly requested to accompany the summary of their articles with the most complete possible keywords.

In order to save time and respect deadlines for publication, it is recommended that authors take care of the complete capture of their article on a computer, and send it to the journal, after they have been informed. acceptance for publication, in the form of files on CD.ROM, which will be copied by the service.

However, since the final formatting of the article is done by P.A.O. (Computer Aided Publication), the authors are asked to avoid any formatting of their text. It will be necessary to avoid stylizing it.

III- Bibliography

The bibliographic references quoted in the text must include only the reference number in square brackets (ex .: [5]). If the name of the author appears in the text, it must be followed by the reference number. When the reference contains more than two authors, only the first is cited, followed by "and al".

For articles, the complete reference includes the names of the authors followed by the initials of their first names, the title of the article, the title of the periodical (in conformity with the abbreviations allowed), the volume, the number of the periodical, the year of publication and the relevant pages.

For the works, the reference must include the names of the authors followed by the initials of their first names, the complete title of the work, the volume, the volume, the first and the last page relating to the results discussed, the number of the edition if there are several, the name of the publisher, the place and the year of edition.

For scientific meetings (congresses, proceedings, ...), the reference includes the names of the authors followed by the initials of their first names, the title of the communication, the identification of the meeting, the place, the period and the pages concerned.

IV- Iconography

Tables, boards, charts, maps, photographs, etc. must be provided separately, inset. They must be presented on white sheets of A4 format, individually or in groups, and have underneath the words "table" or "figure" assigned a number.

The illustrations and figures must be clear, professionally made and adequate for reproduction: a 50% reduction, if any, must lead to a suitable size and thickness of characters for good readability. Moreover, for computer-generated figures, in order to maximize contrast, the use of a laser or inkjet printer is essential.

Legends assigned their numbers must be grouped in a separate page.

The final presentation of the article will be left to the discretion of the Editorial Board.

Journal of Sciences & Technology
Volume 3 N° 1– June 2018

SUMMARY

SUMMARY

Journal of Sciences & Technology
Volume 3 N° 1– June 2018

METHYLENE BLUE MINERALISATION BY ELECTROCHEMICAL PROCESS MEDIATED BY COBALT CATALYST ON PLATINUM ELECTRODES

Submited on 08/07/2015 – Accepted on 27/12/2015

Abstract

In this study, the electrochemical decolorization of the Methylene Blue dye on Platinum electrodes was assessed. Direct oxidation results demonstrate a partial pollutant degradation reaching a maximum of 64 %. However, the addition of a small amount of a redox mediator Co2+/3+ is efficiently able to electrocatalyse the Methylene blue oxidation by shortening significantly the treatment time and enhancing clearly the dye decolorization rate. Nearly complete decolorization was achieved (92 % in 1h 45min). The most striking results achieved within the cyclic voltammetry study demonstrate undoubtedly the pollutant mineralisation. Electrochemical experiments were performed using the spectrophotometric method, which is very convenient, easy and allows monitoring the spectral changes as well as the determination of the dye concentration during the process. The kinetics data show a first-order indirect oxidation kinetics. A mechanism was proposed to explain the different phenomenon during the electrochemical process.

***Keywords**: Decolorization, Methylene Blue, catalyst, Platinum electrode, mineralisation.*

O BRAHMIA [1]
F LOUAFI [2]

1 Laboratory of innovative techniques for the preservation of the environment, Frères Mentouri University, Constantine, Algeria

2 Department of Chemistry, Frères Mentouri University, Constantine, Algeria.

INTRODUCTION :

Methylene Blue (MB) is widely used in biology and chemistry for diverse applications such as; photosensitizer to generate Singlet oxygen, stain for fixed and living tissues, antidote to cyanide and nitrate poisoning (Parry, 1993). In food industry, it is used as optical oxygen sensors. Moreover, it's an organic dye, used to dye cotton, acrylic, silk and wood *(El hajj hassan and El jamal, 2012)*. Generally, dyes are used in various industries such as textile, paint, leather, paper and food *(Hameed and Lee, 2009)*. In the case of textile industry, up to 50 % of the synthetic dyes with different structural varieties such as; azo, diazo, quinine imine, thiazole and others *(Banat and Nigam, 1996)* are lost after the dyeing process and disposal out in the effluents *(Zollinger, 1991)*. Therefore, their elimination from wastewaters is an obligation to prevent the ecosystem destruction. Conventional wastewater treatment based on biological process is not suitably enough to remove recalcitrant dyes from effluents *(Shaul et al., 1991)*. Physical and chemical methods used for eliminating dyes (i.e. adsorption, incineration, electrocoagulation, photocatalysis, ozonation and others) are reasonably effective but relatively cost *(Zhu et al., 2000; Szpyrkowicz et al., 2001)*. That's why; it's necessary to find an effective wastewater method capable of degrading toxic organic compounds from industrial effluents. As alternative, the electrochemical oxidation process is a clean advanced oxidation technology because, the main reagent; the electron, is a clean one *(Jüttner et al., 2000)*. It was applied successfully and proved to be convenient and fruitful to destruct bio-refractory organic compounds due to its high effectiveness and environment well-suited. In the electrochemical oxidation under room temperature and atmospheric pressure, generally, researchers focus their particular interest on the anode oxidation process than the cathode reduction. The Electrochemical methods designed for wastewater treatment consist of direct and indirect oxidation. Mediated Electrochemical Oxidation (MEO) with a redox mediator is considered as one alternative to efficiently remove color from solutions of structurally different dyes. It is as well admitted through this indirect oxidation that a strong oxidative intermediates were generated in situ and consequently convert pollutants into less hazardous products *(Sanromán et al., 2004)*. In this context, we accomplish the MB electrochemical degradation in the presence of $Co^{2+/3+}$ selected as a redox mediator using Pt electrodes. Moreover, it is important to note the conductor behavior of MB, that's why, we achieved this study without any supporting electrolyte to test the feasibility of the MB electrochemical degradation. It should be noted as well that generally dyes are susceptible to undergo a photochemical degradation as they absorb in the visible part of the electromagnetic spectrum, that's why we have worked in the obscurity to avoid any probability of a possible photodegradation pathway. The aim of this work was to test the feasibility of the electrodegradation of MB in our particular conditions. The decolorization rate has been evaluated with and without the redox mediator and the mechanism of the process was suggested in both direct and indirect oxidation.

2. EXPERIMENTAL SECTION

2.1 Materials

Methylene blue (MB) was purchased from Labosi (for analysis) and used without further purification. The cobalt chloride ($CoCl_2$, 6 H_2O) used as redox mediator was purchased from Biochem. Solutions were prepared using distilled water.

2.2 Methods summary :

The electrochemical process was carried out using the spectrophotometric method to follow the dye decolorization. The study was conducted on aqueous solution of MB (3.125 µM), initial pH of 7.8, under atmospheric pressure, at room temperature and in the dark. Experiments were carried out in an electrochemical cell containing the amount of 25 ml of MB for each experiment and using electrodes placed in the cell centre with a distance of 2 cm separating them. The anode and cathode are Pt wire from Voltalab. The ratio electrode surface/volume of dye solution was 0.04 m^2. m^{-3} at laboratory scale. A constant voltage drop of 2 Volt was applied to the electrodes using Potentiostat (Alimentatore per electtroforsi el VI 16, Italy). The reaction vessel was placed on a magnetic stirrer for continuous stirring to ensure the solution homogeneity during the electrochemical process. The conductivity of the initial MB solution was equal to 14.5 µS/cm measured by a conduct-meter model (Inolab Cond 7110). According to this conductor behavior, we choose to perform our experiments without any electrolytes to test the feasibility of the MB degradation in this condition. During the electrochemical process, after each treatment time, we transfer the solution to the UV-visible spectrophotometer (Jenway 6505) to record the absorption spectra of the dye solution and to measure the absorbance at the maximum of MB absorbance (660 nm) using a matched pair of quartz flows cells (1 cm path length). The absorbance data were converted to the concentration using Beer-Lambert (Eq.1). $A = \varepsilon . C . L$ (1), where A and ε are respectively the absorbance and molar absorptivity coefficient values at 660 nm, C is the dye concentration at time t, l is the light path length. The value of ε at 660 nm is deduced from the MB calibration curve, it is equal to 38701 $M^{-1}.Cm^{-1}$. The assays were done twice; the experimental error was below 3 %. The decolorization rate of the dye (Dec %) was expressed as a percentage and calculated by the following (Eq.2). % dye decolorization = $[(C_0 - C_t) / C_0] \times 100$ (2), where C_0 and C_t are the dye concentrations at time 0 and time t respectively. The concentration of the dye was calculated from the absorbance value at 660 nm using a calibration curve. Voltammetric experiments were carried out with a potentiostat model Gamry (USA). The working electrode was a platinum electrode and a reference electrode was a saturated calomel electrode (SCE). All potentials were reported vs. the SCE. A platinum electrode was used as the counter electrode. The scan rate was 100 mV/ s. The experiments were achieved using a cell of 20 ml, we purged the dissolved oxygen by nitrogen bubbling during 25 minutes and we used as 0.1 M of KCl as supporting electrolyte.

3. RESULTS AND DISCUSSION

3.1 Direct oxidation of methylene blue MB

3.1.1 Decolorization rate

To assess the feasibility of the electrochemical process conducted on a solution of methylene blue (3.125 µM) at initial pH of 7.8, we experimentally followed the decolorization by measuring the dye absorbance at its maximum absorption (660 nm) as a function of the different electrochemical treatment time. The decolorization expressed in terms of percentage was calculated according to (Eq.1). The obtained results are shown in (Fig.1). It should be noted that no significant change was observed on the initial pH value of MB during the electrochemical process.

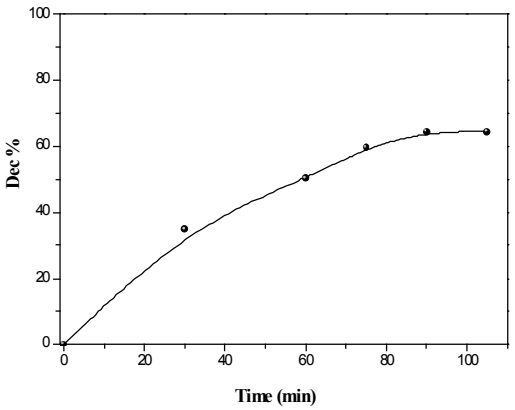

Fig.1. MB decolorization percentage (Dec %) versus the treatment time

Figure.1 indicates a progressive increase of the dye decolorization up to 90 minutes where this last reached a maximum of 64 %. Experiment reveals the gradual disappearance of the blue color which suggests the oxidation of the dye; furthermore, the reaction by-products are colorless. For a treatment time of 105 minutes, the decolorization percentage doesn't change; this leads us thinking about an inhibitory effect against the MB elimination.

3.1.2 Electro-degradation kinetics

To better understand the pollutant behavior, we converted the absorbance to the corresponding concentration and then plotted the pollutant disappearance kinetics (Fig.2).

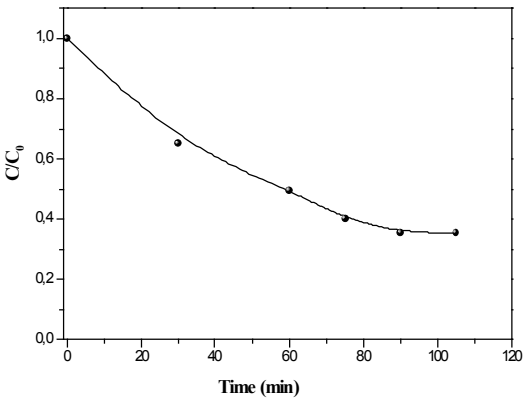

Fig.2. Electrochemical decolorization of Methylene blue (direct oxidation)

According to the plotted curve, it appears two different phases, the first one correspond to a treatment time between 0 and 90 minutes, the elimination rate is rapid at the beginning of the reaction (0,043 µ.mol.l^{-1}.min^{-1}) and the

half-life time is 60 minutes. During this time period, we can readily admit that the reaction proceeds most probably by a transfer of electrons. In other words, the pollutant undergoes anodic oxidation from one hand, since it is capable to give electrons, especially those of the lone doublets of sulfur and nitrogen atoms. On the other hand, we admit a cathodic reduction of water; this last lead to the formation of OH^- anions with the release of H_2 according to the (reaction.1)

$$2\ H_2O + 2\ e^- \rightarrow 2\ OH^- + H_2 \quad (1)$$

We can summarize the proposed mechanism of electro-degradation according to (scheme.1) *(where P and P^+ are respectively the pollutant and the oxidized pollutant).*

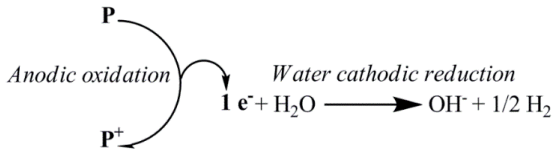

Scheme.1. MB direct oxidation mechanism

The second part of the curve is included between 90 and 105 minutes, we stopped at this end, because the electro-degradation rate no longer changes. This strongly suggests that the intermediates formed during the reaction can compete with the pollutant itself and thus inhibit its elimination. We can generally accept that reactions consuming electrons can limit the MB direct oxidation in solution. All this goes to prove that the direct electrochemical oxidation is only capable to partially oxidize the MB solution, that's why it's interesting to optimize this process to reach the dye total degradation.

3.2 Indirect oxidation :

It's well established that the redox mediators such as ($Fe^{2+/3+}$, $Ce^{3+/4+}$, $Co^{2+/3+}$) are able to generate electrochemically oxidizing species capable of inducing degradation of dyes (Bringman et al., 1995; Farmer et al., 1992). Therefore, it is interesting to consider the redox catalyst effect on MB oxidation. We started our experiment with $Ce^{3+/4+}$ catalyst, no significant change was observed in terms of dye disappearance, this is probably due to its moderate oxidation potential (1.72 V). The second attempt was performed using the couple $Co^{2+/3+}$ with a slightly higher oxidation potential (1.92 V). We tested its effect on MB electro-degradation.

3.2.1 Evolution of MB absorption spectra :

In terms of experimental conditions, the study was performed by adding a solution of $CoCl_2$ (10^{-7} M) to the initial MB solution (3.125 µM), (initial pH 7.8) using the same platinum electrodes. The monitoring of the absorption spectra evolution according to the treatment time between 0 and 105 minutes was accomplished using UV-visible spectrophotometric method. According to (Fig.3), we presented those recorded after 30 and 60 minutes. It clearly appears a decrease in the absorbance at MB maximum absorption (660 nm) in the visible region between (550-750 nm).

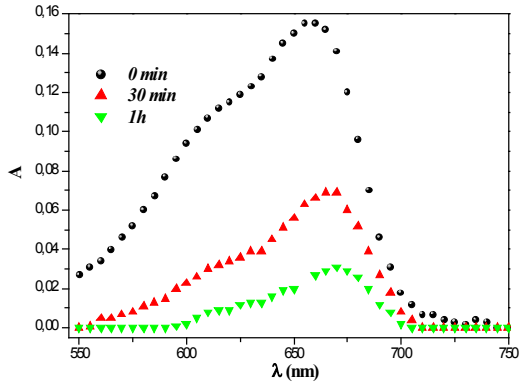

Fig.3. Evolution of the MB absorption spectra during the indirect oxidation

Figure 4 shows properly according to the treatment time, the evolution of the absorbance (A) at 660 nm, which reflects the effective disappearance of the dye and thus our process was significantly optimized by just adding a small quantity of a catalyst.

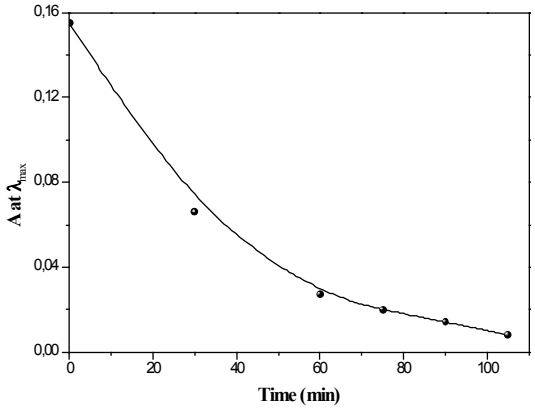

Fig.4. Absorbance evolution (at 660 nm) according to the treatment time

3.2.2 Decolorization rate :

Figure 5 shows the MB decolorization percentage according to the different treatment time during the indirect oxidation.

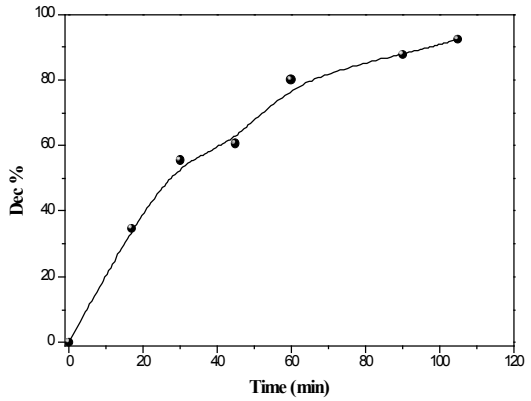

Fig.5. Methylene blue decolorization rate (Dec %) in the presence of Cobalt catalyst

The most important result shows a nearly complete decolorization of 92 % after 105 minutes against 64 % within the direct oxidation. *This reflects the substantial role played by the catalyst in the electrochemical process to increase the dye decolorization percentage.*

3.2.3 Electro-degradation kinetics :

To illustrate the catalyst effect within the indirect oxidation, we have calculated the concentrations from their corresponding absorbances and plotted the kinetics of MB disappearance (C/C_0 versus the treatment time t). (Fig.6)

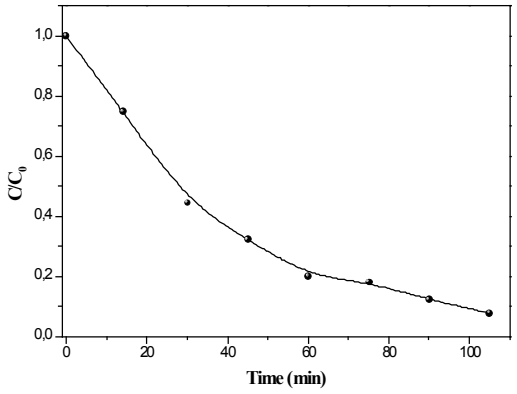

Fig.6. Methylene blue electrochemical decolorization (indirect oxidation)

Figure.6 shows explicitly the dye fast indirect oxidation, the initial rate of disappearance equal to (0.07 µ.mol.l^{-1}.min^{-1}) is 1.62 times faster than the one of the direct oxidation. The half life time is only 28 minutes against 60 minutes in direct oxidation. In other words, the process with the cobalt redox mediator is able to electrocatalyse efficiently the oxidation of MB shortening significantly the treatment time. The superposition of the curves (with and without catalyst) clearly shows these finding (Fig.7).

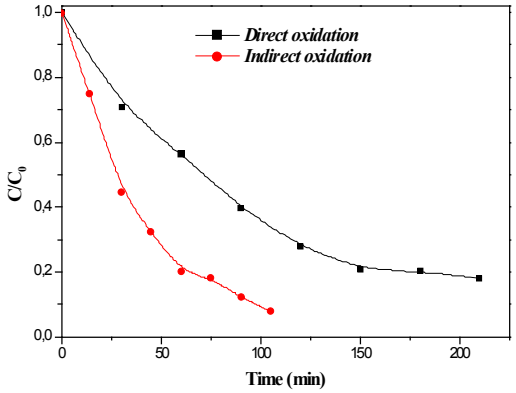

Fig.7. Comparison between the two MB disappearance kinetics (with and without catalyst).

These results demonstrate that the addition of a small amount of cobalt (10^{-7} M) is largely enough to effectively catalyze the MB electrochemical reaction. Furthermore, in terms of reaction kinetics, the indirect oxidation is a first order kinetics. The reaction rate constant is deduced from the curve representing (ln C_0/C versus time) (Fig.8). The plot is linear (R^2 = 0.995) and the rate constant value k is 0.024 min^{-1}.

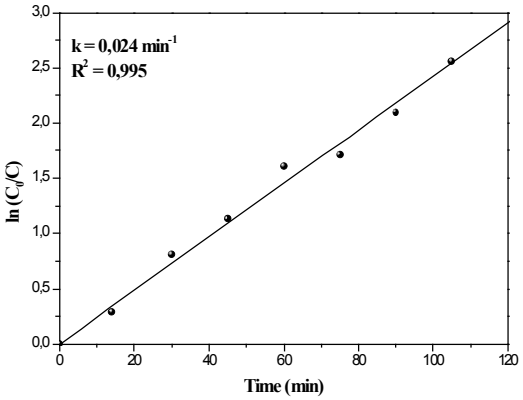

Fig.8. Determination of the rate constant of the MB indirect oxidation.

In this process, metal ions are oxidized anodically from a stable oxidation state to reactive species, which in turn, are capable of oxidizing organic substances to CO_2 (Bringmann et al., 1995). The electro-degradation mechanism is proposed by scheme.2.

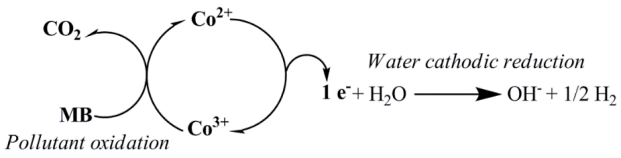

Scheme.2. MB indirect oxidation mechanism

3.2 Cyclic voltammetry :

The cyclic voltammograms (CV) of methylene blue at the potential range -0.8 V to 0.2 V are shown in (Fig.9). The curve (a) on the graph present free MB which yielded one reversible redox system, with the anodic peak potential (E_{ap}) at - 0,148 V, the cathodic peak potential (E_{cp}) at - 0,328 and the peak separation ΔE_p = 1.8 V. In the indirect oxidation, we reached 92 % of MB degradation after 1h 45 min. To guarantee a total MB degradation, we electrochemically treated the solution longer (2h 15 min). The (CV) of this solution was presented on the curve (b). Several conclusions can be deduced; first of all, it appears clearly the complete disappearance of the reversible system found with Free MB; in other words, a complete degradation of the product was observed. Added to this, after a precise search for the apparition of any anodic or cathodic peak, no one was found in the potential range [-2 V, +2 V]. These results provide evidence that all the products yielded from the MB transformation were degraded in their turn. With harmony to these results, we can confirm the mineralisation of the MB dye according to the following reaction: MB (+ e^-) → CO_2 + H_2O. We searched the reduction peak of CO_2 situated at -2.15 V/ CSE according to the following reaction: $CO_2 + e^- \rightarrow CO_2^{\cdot -}$. This peak disappears in our conditions most likely because of the nitrogen bubbling in the solution during all the experiment.

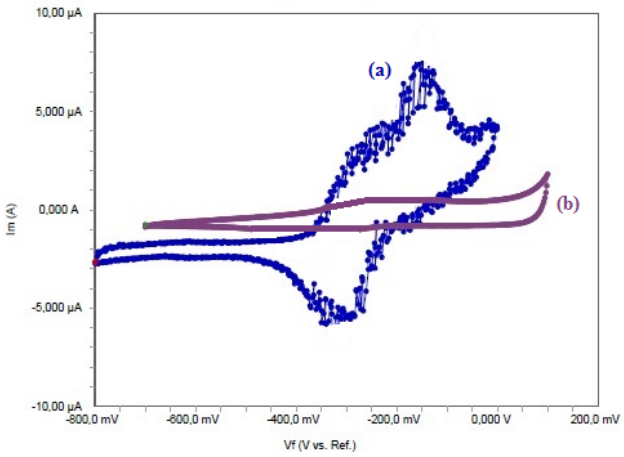

Fig.9. Methylene blue Cyclic Voltammograms, *(a): free MB, (b): MB with cobalt catalyst*

CONCLUSION

The spectrophotometric method was applied successfully on the decolorization of Methylene Blue from aqueous solution by electrochemical process. The results confirm the ability of the direct oxidation to partially oxidize the Methylene blue pollutant. However, a mineralization of the pollutant was obtained by adding a small amount of cobalt redox mediator which increases the decolorization rate and shortens the treatment time. It is noteworthy that the absence of a supporting electrolyte in this study didn't affect the efficiency of the electrochemical process. Added to this, cobalt is not consumed during the process, that's why it can be recovered from the effluent by precipitation or ionic exchange avoiding thus its discharge in the environment.

REFERENCES

- ✓ Bringmann, J., Ebert, K., Galla, U., Schmieder, H., 1995. Electrochemical mediators for total oxidation of chlorinated hydrocarbons: formation kinetics of Ag (II), Co (III) and Ce (IV). J. Appl. Electrochem. 25, 846-851.
- ✓ Banat, I.M., Nigam, P., 1996. Microbiol decolorization of textile dyes containing effluents. A review. Bioresource. Technology. 58, 217-227.
- ✓ Hameed, B.H., Lee, T.W., 2009. Degradation of malachite green in aqueous solution by fenton process. J. Hazard. Mater. 164, 468-472.
- ✓ Jüttner, K., Galla, U., Schmieder, H., 2000. Electrochemical approaches to environmental problems in the process industry. Electrochim. Acta. 45, 2575-2594.
- ✓ Farmer, J.C., Wang, F.T., Lewis, P.R., Summers, L.J., 1992. Electrochemical treatment of mixed and hazardous wastes: oxidation of ethylene glycol by cobalt (III) and iron (III). Process Saf. Environ. Prot. 70, 158-164.
- ✓ Parry R.T., 1993. Principles and Applications of Modified Atmosphere Packaging of foods, Parry RT editor, Blackie Academic Press, London.
- ✓ Shaul, G.M., Holdsworth, T.J., Dempsey, C.R., Dostall, K.A., 1991. Fate of water soluble azo dyes in the activated sludge process. Chemosphere. 22, 107-119.
- ✓ Szpyrkowicz, L., Juzzolino, C., Kaul, S.N., 2001. A comparative study on oxidation of disperses dyes by electrochemical process, ozone, hypochlorite and Fenton reagent. Water. Res. 35, 2129-2136.
- ✓ Sanromán, M.A., Pazos, M., Ricart, M.T., Cameselle, C., 2004. Electrochemical decolourisation of structurally different dyes. Chemosphere. 57, 233-239.
- ✓ Zollinger, 1991. Color Chemistry: Syntheses, properties and Applications of Organic Dyes and Pigments, VCH Publishers. Weinheim, Germany.
- ✓ Zhu, C., Wang, L., Kong, L., Yang, X., Zheng, S., Chen, F., Maizhi, F., Zong, H., 2000. Photocatalytic degradation of AZO dyes by supported TiO_2 + UV in aqueous solution. Chemosphere. 41, 303-309.

THE EFFECT OF THE THERMAL INERTIA ON THE TEMPERATURE OF A HEATING SLAB.

Submited on 18/12/2013 – Accepted on 24/08/2014

Abstract

The paper presents the influence of the thermal inertia on the temperature of a heated concrete slab. This is a solar sensor provides a solar heating system floor, which the energy input.

The concept of thermal inertia is not easy to grasp. It is defined as the speed that helps a system ((building in our case) reacts to the change in operating conditions. The response of the building facing to the stresses is largely depending on the thermal properties of constituent materials. This feature is related to good performance, good use, and comfort of the thermal machine which is called ''habitat''.

The objective of this work aims to study the influence of the inertia on the surface temperature of the floor, to design the future of homes with high inertia and very low energy consumption with satisfactory comfort conditions.

Keywords: *thermal inertia, solar heating, solar collector, floor, Forte inertia habitat.*

D ABBAZ
A CHAKER

Energy Physics Laboratory, Frères Mentouri University, Constantine, Algeria.

I. INTRODUCTION:

Today, theconstruction industrygoes into anew era.The energyconsumption of buildingsrepresentingAlgeria,almost 47%of the energy producedand they are responsible forover 25%of greenhousegas emissionsmust be reducedby economic andenergy solutionsrespect to the environment.
For this, improving the building's envelope which is reinforced by insulationand better treatmentof thermal bridgeswhich introduce lower thermal requirementsinair conditioning andheatingshould be taken into consideration. Further research should focus on efficient building heating systems to control the atmosphere of living with a lower energy cost. Certainly, maintenaning the atmosphere is entrusted to the heating system whose quality depends greatly on the design, the design and implementation of the facility. At the same time, technological development in the field ofcurrent heatingneeds to go parallel to the direction ofreducing thenegative environmental impactthrough the use ofrenewable energy sources and toensure also the securityof ourenergy suppliesfacingthe depletion offossil energy resources.

Inthis approach, theheated floorhas a particular placein technology. Itprovides optimalheat distributionvertically and horizontally,perfectly compatible withrenewable energy sources. it is one oflow temperaturesystemswhichreduces theenergy consumption through its use.

Research has been under taken on this heating technology and several designs were studied .A.Mokhtariet al(1992) demonstrated in atheoretical and experimental studyof astorage room witha directsolar flooracaptureratio of 8to 10%ismore than enoughaccordingtothe Algerianclimate.The authorsalso notedthat asensor surfaceequal to 10%ofthe heating floor's surface can be usedwithout fear ofoverheating[1].

For the dimensions that are suitable for our climate, and to avoid the overheating phenomenon and have some thermal comfort. Kharchi A. (2000), used a report in his experimental study, capture area / exchange area (slab) equal to 0.5, for a slab thickness of 10 cm above the grid [2].

II. THEHEATING SYSTEM

A directsolar floorconsists essentiallyof three elements:

●The solar panel capturesthat convert transformsunlight into heat.

●A slabwherein in whichthe heat transferfluidheatedby the sensors.The lattersimultaneouslyserves to storetheheat generatedby the sensors andtothereturnin the same wayas a conventionallow-temperaturefloor heating, but with a certaintime lag.

●A transfergroup that managesthe heating of thePSD[3].

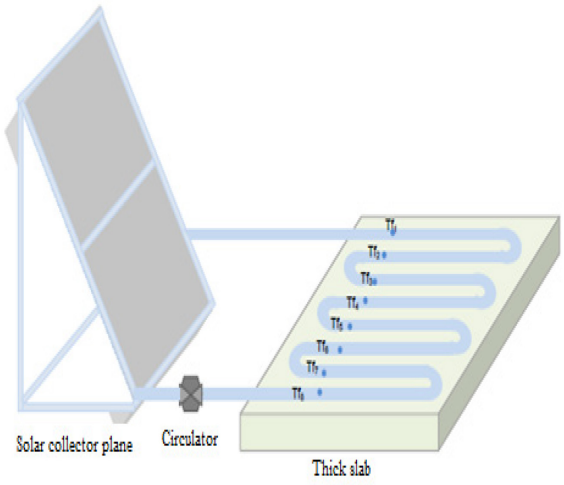

III. MATHEMATICALFORMULATIONSYSTEM

The systemis modeledaccording tonodalmethod, based ontheheat balancesofeachelement which constitutestheheating system: sensor, coolant, floorconsisting ofa concrete slab.

A. Simplifying assumptions

- The physical properties of materials are assumed to be constant.
- The flow regime is transitional.
- The different solid media have a uniform temperature in a plane normal to the direction of flow.
- The heat flows are of one-dimension.
- The heat transfer fluid used is a pure water.
- the heat losses between the solar collector and the floor are negligible.
- The temperature of the water leaving the solar collector is equal to that of the water at the inlet of the under floor heating.
- We limit ourselves only to study the exchange of heat from the top of the coil (the floor is well isolated from the ground side).
- The heat transfer fluid circulates on the velocity u in the tube.
- The floor temperature isconsidereduniform.

B. Heat balance

1) Usefulpower recoveredby the fluid

The useful power recovered by the heat transfer fluid is governed by the equation [4], [5]:

$$P_u = F_R \cdot \left((\tau\alpha)_{eff} \cdot P_g - U_g \cdot (T_{fe} - T_a)\right) \cdot S_c \quad (1)$$

Or :

$(\tau\alpha)_{eff}$: Effective coefficient ofabsorption.

F_R :Overall efficiency of thethermalexchangeof the sensor.

T_{fe} :Entered temperatureof the coolant.

P_g : Overall power.

U_g :overall heat loss.

2) Heat balanceat thehotslab

By performingaheat balanceat eachnode, we obtain a system of twoequations describingthebehaviorof thefloor.

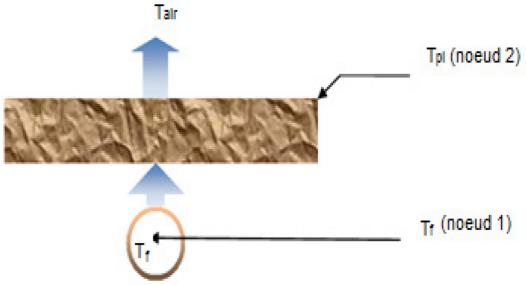

Fig.2.Nœudsconsidered in thefloor

- Nœud1 : (the heat transfer fluid)

$$M_f Cp_f \frac{\partial T_f}{\partial t} + U_f Cp_f \frac{\partial T_f}{\partial y} = h_{vplf} S_{plf} (T_{pl} - T_f) + h_{cplf} S_{pl} (T_{pl} - T_f) \quad (2)$$

Dividing by$M_f.Cp_f$, we obtain:

$$\frac{\partial T_f}{\partial t} + \frac{V_f V_{fmax}}{M_f} \frac{\partial T_f}{\partial y} = \frac{h_{vplf} S_{plf}}{M_f Cp_f} (T_{pl} - T_f) + \frac{h_{cplf} S_{pl}}{M_f Cp_f} (T_{pl} - T_f) \quad (3)$$

- Nœud 2: (the floor)

$$\frac{dT_{pl}}{dt} = \frac{h_{vplf} S_{plf}}{M_{pl} Cp_{pl}} (T_f - T_{pl}) - \frac{S_{pl}}{M_{pl} Cp_{pl}} (\varphi_{vpla} + \varphi_{rpl}) \quad (4)$$

With:

φ_{rpl} : Exchangeradiantwith air.

φ_{vpla} : Exchangeconvectionwith air.

Thisequationcompletedby the initial conditionsandsystemboundary, formsasystem of nonlinearequationsandcoupled. The resolutionis performed bythe finite differencemethodusing thedescendingimplicit schemeforthe convectivetermfluidandan explicit schemeforthetransientterm.

IV. RESULTS AND DISCUSSION

The thermal inertiaimposes a certaintime delaybetween the moment whenthe water isintroduced into the tubeand the temperature of thesurface varies.

Thethermalinertia associated with conduction'sphenomenondepends on the thicknessof the slab andthethermo physicalcharacteristics of the materials which consist of (volume, massthermal conductivity, thermal emissivity) [2].

A. Temporal variation inuseful powerof the sensor

It is evident thatthe usefulpower recoveredby the fluidclosely depends on theglobal solar radiation. Thus, andas shown inFigure 3, theusefulpower(heat supplied to the floor) has a bell shape,itis between 120and300watts.

This result has a good agreement withwhat was found inthe literature [2].

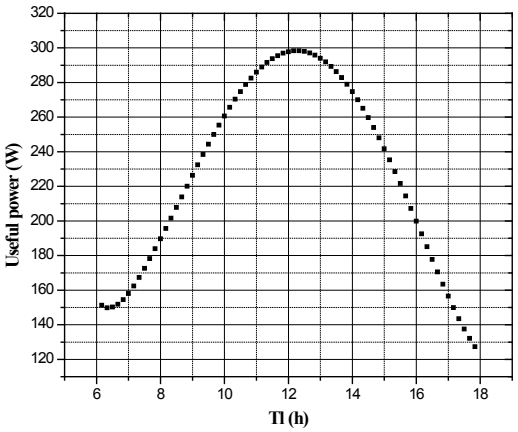

Fig .3. Variationtemporalofthe useful power of the sensor

B. Assessment of the roleof inertiaonthe floortemperature:

1) Influence of the thickness of theconcrete:

a)-Effect ofthe thickness of theconcreteonthe floor temperature:

Figure4.a illustrates the evolution ofthe flour's maximum temperature as a function oftimefordifferent thicknesses of the concrete's layer.It is clear thatthemaximum temperature of thefloordecreases when the thicknessof the layer ofconcrete increases.

Thefloor temperaturewill be evenweaker thanthe concrete massis important.

b) Effect ofthe thickness of theconcreteover the usefulpower:

In Figure4.bwe canfind that theconsumptionof useful powerdecreases when thethickness of the upperconcrete layeris increased (the thermal losses between the sensor andtheslabbeing assumednegligible,theheattransferred totheslabisthusequal to the energycaptured by the"power output" sensor).

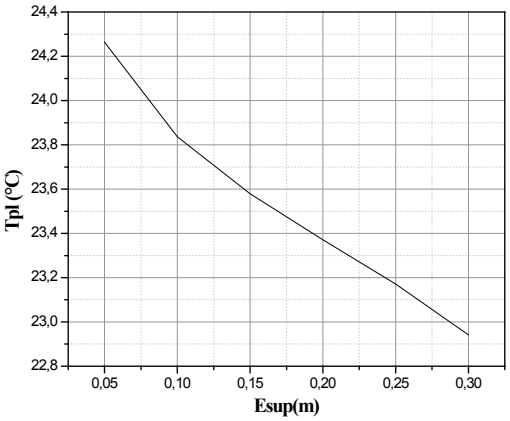

Fig .4 .(a) Influence of the thicknessof the concreteonthe floor temperature.

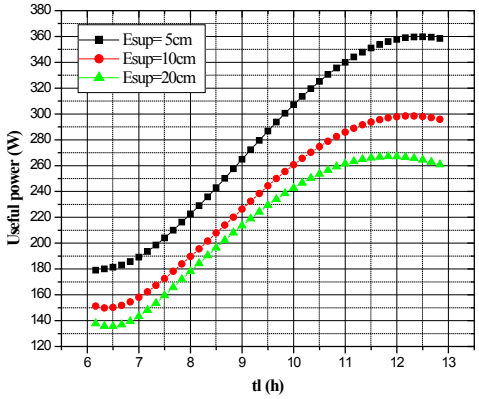

Fig .4.((b) Effectof the thickness ofthe top layer of the useful power .

2) Influence of the thermal resistance of concrete

It is evident thatthefloor's temperatureis highly dependent onthe thermal resistance ofthe top layer ofconcrete.Thus, andasseen in Figure5, the increasing of the thermal's resistance ofconcreteleads to lower of theheat exchange with theatmosphere which directs to areductionofthe floor temperature.

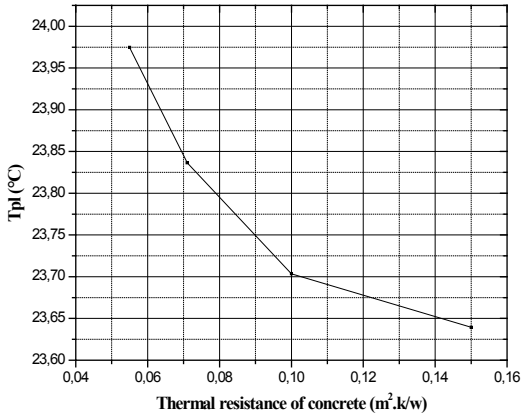

Fig .5. Evolution of thefloor temperatureinfunctionofthe thermal resistance ofthe top layer ofconcrete

3) Influence of emissivity of concrete

The examination of thecurves in Figure6allowssaying thatthefloor temperatureismoreimportant in the casewheretheradiation is nottaken into consideration;in this casethe amount of heattransferred tothe air will beconsiderably larger.

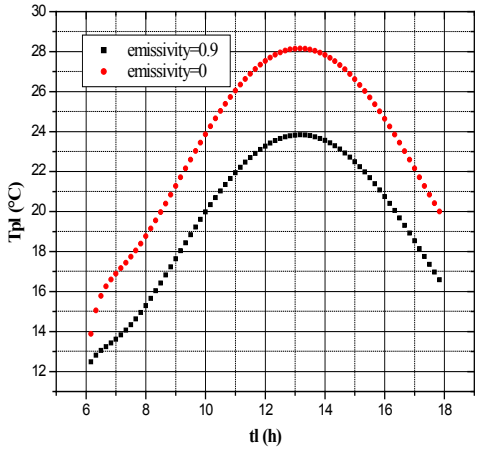

Fig .6. Temporal evolutionofthe temperature of aradiant floorand a nonradiant floor

CONCLUSION

Thermal inertiais thus acomplex phenomenon. Multiple criteriashould be taken into account to forobtaining thesame comfortfor lessconsumption.

The result of the study conducted the following conclusions:

The inertia of thefloorisdirectlyrelated to the thicknessoftheconcretelayer located above heating pipes. With this configuration,it has been shownthatthefloor temperaturewas evenlower thanthe concretemassincreased.

Therefore, it is recommended to increase as much as possible the thickness of the top layer of concrete. Nevertheless, we cannot afford to have too thick floor. Indeed, the "National Building Code" sets the minimum thickness of concrete floors of homes to 75 mm for the slab itself, and the use of a greater thickness is not necessary. A slab 10 cm thick may be a compromise quite interesting.

Furthermore,the natureof the floor coveringaffects the thermalpower emitted by thefloorandonitssurface temperature.

REFERENCES

[1] A.Mokhtari, KazeouiH., Y. Boukezzi, G. Achard. Use of ahydraulic circuitin a floorfor heatingand coolingof premises.Journalof renewablesvol 1, 17-27(1998).

[2] R. Kharchi, N. AitMessaoudeneMr.Belhamel. Experimental studyof the thermal behaviorof a directsolar floor.Journalof Renewable Energies, International DaysofThermal (2002).

[3] R. Kharchi. Experimental studyof the thermal behaviorof a directsolar floor.MagisterthesisBlidaUniversity(2002).

[4] M. Boubekri, ShakerA., A. Cheknane. NumericalapproachforperformancestudyofhybridPV /thermalcollector.Revuerenewable energyvol 12, No. 3 (2009).

[5] M. E.A.Bekkouche. Modelingthe thermal behaviorof a fewsolar devices.PhD thesis,University of Tlemcen(2009)..

[6] P. Friedman.The heatingand refreshingfloor, regulation, design, implementation, adjustment.ParisienneEdition(2003).

3D NUMERICAL STUDY OF FLOW IN A SOLAR CHIMNEY POWER PLANT SYSTEM

Submited on 12/03/2014 – Accepted on 04/12/2014

Abstract

Heat transfer process and fluid flow in a Solar Chimney Power Plant System (SCPPS) are investigated numerically. As simulation object we use the Spanish prototype plant. The calculative model and boundary conditions in calculation are introduced. Boussinesq model was chosen in the natural convection processus, Discrete Ordinate radiation model was employed for radiation. The principal factors that influence on the performance of the Solar Chimney have been analysed. The effects on the flow of the Solar Chimney which caused by solar radiation intensity have been simulated. The calculated results are compared and are approximately equivalent to the relative experimental data of the Manzanares prototype. It can be concluded that the temperature difference between the inlet and outlet of collector, as well as the air velocity in the collector of the system, is increase with the increase of solar radiation intensity and the pressure throughout system is negative value.

Keywords: *Terms—Solarchimney power plant, Numerical simulation, solar radiation intensity, Flow characteristics.*

T TAYEBI
M DJEZZAR
H GOUIDMI

Energy Physics Laboratory, Department of Physics, Faculty of Science, Frères Mentouri University, Constantine, Algeria.

I. INTRODUCTION

The Solar Chimney Power Plant System (SCPPS) is a natural driving power generating system. It can convert solar energy first into thermal energy then into kinetic energy finally into electrical power. The concept was first suggested by Günther in 1931 and again by Schlaich [1] in 1978. Subsequently a prototype of a solar chimney with a height of 194.6m and collector area of radius 122 m was constructed at Manzanares, (Spain) and data of actual working of the solar chimney was collected [1]. Schlaich reported the nominal electric power output at Manzanares to be 50 KW.

As the solar chimney, power plant systems could make significant contributions to the energy supplies of those countries where there is plenty of desert land, which is not being utilized, and sunlight available in Africa, Asia and Oceania, researchers have made many reports on this technology in the recent few decades.

Haaf et al. [2] provided fundamental investigations for the Spanish prototype system in which the energy balance, design criteria, and cost analysis were discussed. The next year, the same authors reported preliminary test results of the solar chimney power plant [3].

Zhou Xinping [4] presented experiment and simulation results of a solar chimney thermal power generating equipmentin China, and based on the simulation and the specific construction costs at a specific site, the optimum combination of chimney and collector dimensions was selected for the required electric power output. Ming et al. [5] presented a thermodynamic analysis of the solar chimney power plant and advanced energy utilization degree to analyze the performance of the system, which can produce electricity day and night. Ming et al. [6] developed a comprehensive model to evaluate the performance of a solar chimney power plant system in which the effects of various parameters on the relative static pressure, driving force, power output and efficiency have been further investigated. The authors supposed the existing models are insufficient to accurately describe all the phenomena occurring in solar chimney power plant. Using the solar chimney prototype of Manzanares, as a practical example, 3D turbulent flow numerical simulation studies were performed to explore the geometrical modifications on the system performance. Results showed a good agreement with the analytical model. The control of the SCPP analytical tools such as dynamic simulation of these systems is essential. Ming et al. [7] to analyze the characteristics of heat transfer and airflow in the solar chimney power plant system with energy storage layer. Different mathematical models for the collector, the chimney and the energy storage layer were established, and the effect of solar radiation on the heat storage characteristic of the energy storage layer was analyzed. Numerical simulation results show that the heat storage decreases firstly and then increases with the increase of the solar radiation from 200W/m2 to 800W/m2. The static pressure decreases while the velocity increases significantly inside the system with the increase of solar radiation; the average temperature at the outlet of the chimney and the one of the energy storage layer may increase too significantly with the increase in solar radiation. In addition, the temperature gradient of the storage medium may increase and this results in an increase of energy loss from the bottom of the energy storage layer. Pastohr et al. [8] used the FLUENT software for modeling a solar chimney power plant, geometrically similar to that of Mansaranes, with the aim of carrying out an analysis and reporting details on the operating mode and the system efficiency. They confirmed that the pressure drop in the turbine and the mass flow rate, decisive elements on the system effectiveness, cannot be only given by coupling all the parts of a SCPP. Numerical results given by FLUENT software are in good agreement with the results given by a

simple model proposed by the authors, which led to the conclusion that it is much easier to use it for parametric studies. Chergui et al. [9,10] simulated a thermohydrodynamicbehaviour analysis of the airflow through an axisymmetric system, such as chimneys, with defined boundary conditions.

II. MODELING

a. Geometric Mode

The three-dimensional geometric model of the SCPPS was built in GAMBIT, which is a pre-processor of FLUENT. The grid was also generated in GAMBIT [11]. The collector is 240m in diameter, and the distance between its covering and ground surface is 1.7m, the chimney is 200m in height and 10m in diameter.

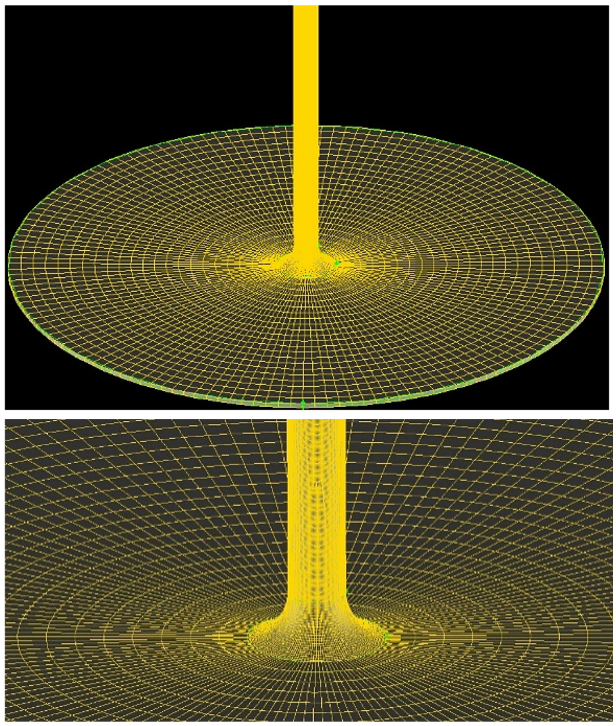

Fig.1 Grid model of the whole system

III. MATHEMATICAL MODEL

Based on the geometrical dimensions of the prototype Manzanares,a physical model for a solar chimney power plant was built. The basic equations including the models were numerically solved with the help of the commercial simulation program FLUENT [12]. The control equations including the continuity equation, momentum equation, energy equation, and turbulence equation (the standard k–ε equations) in the collector and chimney regions can be written as follows:

Continuity equation

$$\frac{\partial \rho}{\partial t}+\frac{\partial(\rho u)}{\partial x}+\frac{\partial(\rho v)}{\partial y}+\frac{\partial(\rho w)}{\partial z}=0 \qquad (1)$$

Navier-Stokes equation

$$\frac{\partial(\rho u)}{\partial t}+\frac{\partial(\rho uu)}{\partial x}+\frac{\partial(\rho uv)}{\partial y}+\frac{\partial(\rho uw)}{\partial z} = -\frac{\partial p}{\partial x}+\mu\left(\frac{\partial^2 u}{\partial x^2}+\frac{\partial^2 u}{\partial y^2}+\frac{\partial^2 u}{\partial z^2}\right) \qquad (2)$$

$$\frac{\partial(\rho v)}{\partial t}+\frac{\partial(\rho vu)}{\partial x}+\frac{\partial(\rho vv)}{\partial y}+\frac{\partial(\rho vw)}{\partial z} = -\frac{\partial p}{\partial y}+\mu\left(\frac{\partial^2 v}{\partial x^2}+\frac{\partial^2 v}{\partial y^2}+\frac{\partial^2 v}{\partial z^2}\right) \qquad (3)$$

$$\frac{\partial(\rho w)}{\partial t}+\frac{\partial(\rho wu)}{\partial x}+\frac{\partial(\rho wv)}{\partial y}+\frac{\partial(\rho ww)}{\partial z} = -\frac{\partial p}{\partial z}+\mu\left(\frac{\partial^2 w}{\partial x^2}+\frac{\partial^2 w}{\partial y^2}+\frac{\partial^2 w}{\partial z^2}\right) + \rho g\beta(T-T_0) \qquad (4)$$

Energy equation

$$\frac{\partial(\rho cT)}{\partial t}+\frac{\partial(\rho cuT)}{\partial x}+\frac{\partial(\rho cvT)}{\partial y}+\frac{\partial(\rho cwT)}{\partial z} = \lambda\left(\frac{\partial^2 T}{\partial x^2}+\frac{\partial^2 T}{\partial y^2}+\frac{\partial^2 T}{\partial z^2}\right) \qquad (5)$$

k–ε equations

$$\frac{\partial(\rho k)}{\partial t}+\frac{\partial(\rho ku)}{\partial x}+\frac{\partial(\rho kv)}{\partial y}+\frac{\partial(\rho kw)}{\partial z} = \frac{\partial}{\partial x}\left(\left(\mu+\frac{\mu_t}{\sigma_k}\right)\frac{\partial k}{\partial x}\right) + \frac{\partial}{\partial y}\left(\left(\mu+\frac{\mu_t}{\sigma_k}\right)\frac{\partial k}{\partial y}\right) + \frac{\partial}{\partial z}\left(\left(\mu+\frac{\mu_t}{\sigma_k}\right)\frac{\partial k}{\partial z}\right)+G_k+G_b-\rho\varepsilon + S_k \qquad (6)$$

$$\frac{\partial(\rho\varepsilon)}{\partial t}+\frac{\partial(\rho\varepsilon u)}{\partial x}+\frac{\partial(\rho\varepsilon v)}{\partial y}+\frac{\partial(\rho\varepsilon w)}{\partial z} = \frac{\partial}{\partial x}\left(\left(\mu+\frac{\mu_t}{\sigma_\varepsilon}\right)\frac{\partial \varepsilon}{\partial x}\right) + \frac{\partial}{\partial y}\left(\left(\mu+\frac{\mu_t}{\sigma_\varepsilon}\right)\frac{\partial \varepsilon}{\partial y}\right) + \frac{\partial}{\partial z}\left(\left(\mu+\frac{\mu_t}{\sigma_\varepsilon}\right)\frac{\partial \varepsilon}{\partial z}\right) + C_{1\varepsilon}G_k + C_{1\varepsilon}C_{3\varepsilon}G_b - C_{2\varepsilon}\frac{\rho\varepsilon^2}{k}+S_\varepsilon \qquad (7)$$

G_k : represents the generation of turbulence kinetic energy due to the mean velocity gradients;

G_b : is the generation of turbulence kinetic energy due to buoyancy.

The constants have the following values [13]:

$C_{1\varepsilon}=1.44, C_{2\varepsilon}=1.92, C_\mu=0.09,\ \ \sigma_k=1, \sigma_\varepsilon=1.3.$

a. Boundary Conditions:

Settings of boundary conditions are shown in TABLE I. Pressure boundary condition was used to simulate the natural convection flow in the actual system. DO radiant model and convection heat transfer boundaries were used in this study (considering that air, has the heat transfer medium in the system, as thin optical thickness). The ground under collector covering roof that absorbs solar energy can be seen as a local heat source ($q_0 = G.\tau.\alpha$ W/m^2). Ambient temperature T_0 is set at 293 K, the ground absorptivity is $\alpha = 0.9$ and the glass roof transmissivity is $\tau = 0.9$. Solar radiation intensity Ghas been changed.

TABLE I:The main boundary conditions

Place	Type	Value
The ground	Wall	$q_0 = G.\tau.\alpha$ (inner heat source)
Surface of the chimney	Wall	$q = 0$ W/m^2
Glass roof	Wall	h=8W/(m^{2}K), $T_0 = 293K$
Collector inlet	Pressure inlet	$T_0 = 293K, \Delta P = 0$ Pa
Chimney outlet	Pressure outlet	$\Delta P = 0$ Pa

IV. RESULTS AND DISCUSSION

All numerical calculations had to be performed with the solver with double precision. The iteration error was at least 10^{-4} for all calculations, and was at least 10^{-6} for the energy equation. The solution converged in less than 600 iterations.

Figures 2–4 illustrate the temperature, velocity and pressure distributions in the solar collector of the solar chimney power plant at three different solar radiations.

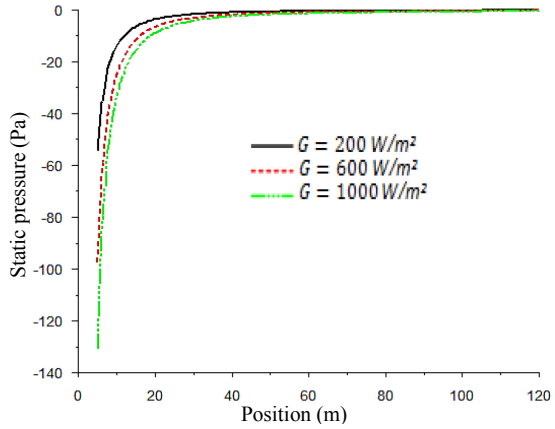

Fig.2 Static pressure profile of the fluid flowing through the collector.

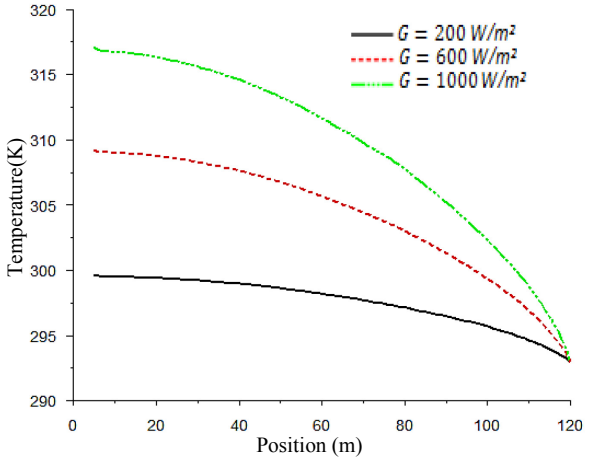

Fig.3 Temperature profile of the fluid flowing throughthe collector.

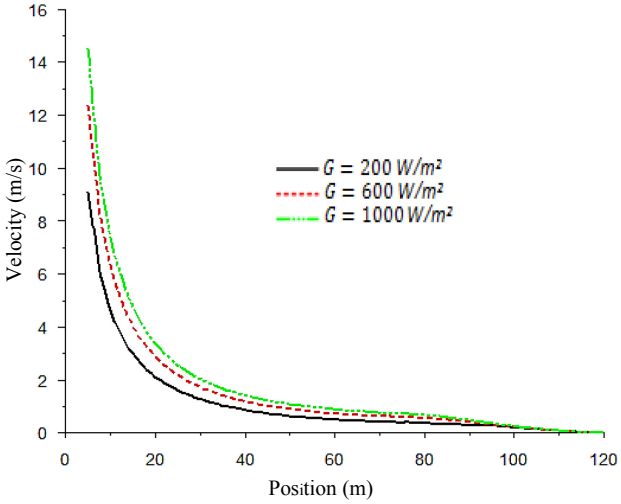

Fig.4 Velocity profile of the fluid flowing through the collector.

Figure 2 shows the static pressure profile, which decreases through the collector and drops dramatically near the chimney base. It also demonstrates that when the collector radius is constantthe increasing in solar radiation results in a decrease in the static pressure.

Figure 3 illustrates that, when the solar radiation intensity increases, the air temperature increases for the same collector radius and when the solar radiation is constant, the temperature of fluid increases by decreasing the radius.

The velocity increases through the collector by decreasing the radius, but it increases more sharply by reaching the chimney base. When the collector radius is constant, an increase of solar radiation causes an increase of the air velocity, but the effect is not very significant (see Fig.4).

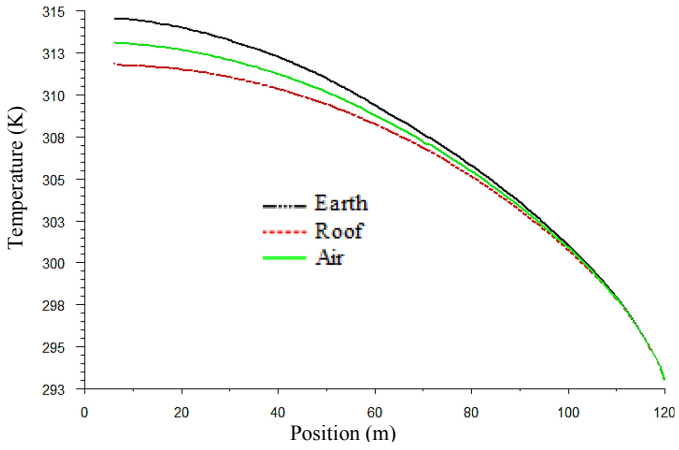

Fig.5 Temperature profiles of the earth, roof and air through the collector for $G=800$ W/m^2.

Figure5 illustrates the earth, roof and air temperature profiles through the collector. As shown in Figure 5, by decreasing the collector radius, all the temperatures increase, but the earth temperature increases more steeply.

TABLE II. Results of calculations for different solar radiations.

Solar radiation G (W/m^2)	Temperature difference between the inlet and outlet of collector (K)	Air velocity at outlet of collector (m/s)	Pressure difference between the inlet and outlet of collector (Pa)
200	6.62	9.10	54.343
400	11.77	10.97	77.86
600	16.25	12.37	97.58
800	20.31	13.52	115.04
1000	24.07	14.61	130.89

Simulative results (See Table II) show the relations between solar radiation intensity and three main parameters, including the differential pressure of collector, the air velocity of chimney base and the temperature difference between the inlet and outlet of collector. These three main parameters increase with the increasing solar radiation intensity. It's the reason that the SCPPS is always built in the countries or areas of which much more in annual mean sunshine.

To validate the numerical results, the temperature increase in the collector was compared with the experimental data of the Spanish prototype for 1000 w/m^2 [2]. As is shown in TABLE III, an acceptable quantitative agreement was obtained between the experimental data of the Manzanares prototype and both of the numerical results.

TABLE III. Comparison between the numerical results and the experimental data.

Results	Temperature increase	Air velocity at outlet of collector
Experimental data from Manzanares	20K	15 m/s
Our work	24.07K	14.61 m/s

V. CONCLUSION

A numerical simulation was performed with the help of FLUENT to analyze the characteristics of the flow for the geometry of the prototype in Manzanares, Spain, and both results are consistent with the experimental data of the Manzanares prototype. Numerical profiles for the temperature, velocity and pressure in the collector of the solar chimney power plant were shown for different solar radiations. It can be concluded that the pressure throughout system is negative value. The temperature difference between the inlet and outlet of collector is increase with the increase of solar radiation intensity, and increases by decreasing the radius. The velocity increases through the collector by decreasing the radius, and also an increase of solar radiation causes an increase of the air velocity. The calculated results are approximately equivalent to the relative experimental data of the Spanish prototype.

REFERENCES

[1] Schlaich J. The solarchimney: electricityfrom the sun, edition axel menges. Germany: Geislingen; 1995.
[2] Haaf W, Friedrich K, Mayer G, Schlaich J. Solar chimneys. Int J Sol Energy 1983;2:3–20.
[3] Haaf W, Friedrich K, Mayer G, Schlaich J. Solar chimneys. Int J Sol Energy1984;2:141–61.
[4] Xinping Zhou, et al. Simulation of a pilot solarchimney thermal power generatingequipment. RenewEnergy 2007; 32:1637–44.
[5] Ming TZ, Liu W, Xu GL, Yang K. Thermodynamicanalysis of solarchimney power plant system. J HuazhongUnivSciTechnol 2005; 8:1–4.
[6] Ming TZ, Liu W, Xu GL. Analytical and numerical investigation of the solarchimney power plant systems. International Journal of EnergyResearch 2006; 30:861–73.
[7] Ming TZ, Liu W, Pan Y, Xu GL. Numericalanalysis of flow and heattransfercharacteristics in solarchimney power plants withenergystorage layer. Energy Conversion and Management 2008; 49:2872–9.
[8] Pastohr H, Kornadt O, Gurlebeck K. Numerical and analyticalcalculations of the temperature and flow field in the upwind power plant. International Journal of EnergyResearch 2004; 28:495–510.
[9] Chergui T, Larbi S, Bouhdjar A, Gahgah M. Heattransfermodellinganalysis of flows in solarchimneys. In: Proceedings of the fourth international conference on computationalheat and mass transfer; 2009.
[10] Chergui T, Larbi S, Bouhdjar A, Gahgah M. Influence of the thermohydrodynamic aspect of fluid flow on the performance analysis of a solarchimney power plant. In: Proceedings of the world renewableenergycongress 2009—Asia; 2009.
[11] FLUENT Inc., GAMBIT Modeling Guide, Fluent Inc., 2003.
[12] Fluent Inc., 2005. Fluent 6.3 User Guide.

NUMERICAL STUDY OF THE MIXED CONVECTION HEAT TRANSFER IN ANNULUS HEATED BY JOULEAN EFFECT

Submited on 12/05/2014 – Accepted on 24/06/2014

Abstract

In the present work, we numerically study the three-dimensional mixed convection heat transfer in the annular space between tow concentric horizontal pipes, the external pipe is heated by an electrical intensity passing through its small thickness while the inner cylinder is insulated. The convection in the fluid domain is conjugated to thermal conduction in the pipes solid thickness. The physical properties of the fluid are thermal dependant. The heat losses from the external outside pipe surface to the surrounding ambient are considered. The model equations of continuity, momenta and energy are numerically solved by a finite volume method with a second order spatiotemporal discretization. The obtained results show the three dimensional aspect of the thermal and dynamical fields with considerable variations of the viscosity and moderate variations of the fluid thermal conductivity. As expected, the mixed convection Nusselt number becomes more superior to that of the forced convection when the Grashof number is increased. At the solid-fluid interface, the results show clearly the azimuthal and axial variations of the local heat flux and the local Nusselt numbers. Following these results, we have tried modelling the average Nusselt number Nu_A as a function of Richardson number*Ri*. With the parameters used, the heat transfer is quantified by the correlation: $Nu_A = 9.9130\ Ri^{0.0816}$.

Keywords: *Mixed Convection, Annulus, Conjugate Heat Transfer, Numerical simulation.*

S TOUAHRI
T BOUFENDI

Physic Energetic Laboratory, Department of Physic, Faculty of Science, Frères Mentouri University, Constantine, Algeria.

I. NOMENCLATURE

D_{1i}	Internal diameter of inner pipe, [m].
D_{1o}	External diameter of inner pipe, [m].
D_{2i}	Internal diameter of outer pipe, [m].
D_{2o}	External diameter of outer pipe, [m].
D_h	Hydraulic diameter, [m].
I	Electrical intensities, [A].
L	Pipe length,[m].
g	Gravitational acceleration, (= 9.81), [m·s^{-2}]
G	Volumetric heat generation, [Wm^{-3}]
G^*	Non-dimensional volumetric heat generation, $\left(K_S^* / \mathrm{Re}_0 \mathrm{Pr}_0\right)$.
Gr^*	ModifiedGrashof number, $(= g\beta G D_i^5 / K_s \nu^2)$
h_r	Radiative heat transfer coefficient, [W/m^2·°K].
h_c	Convective heat transfer coefficient, [W/m^2·°K].
K^*	Nondimensionalthermal conductivity, (K/K_0).
K_0	Fluid thermal conductivity at the entrance, [W/m·°K].
K_s	Pipe thermal conductivity, [W/m·°K].
$Nu\ (\theta, Z^*)$	Local Nusselt number.
$Nu\ (Z^*)$	Axial Nusselt number.
Nu_A	AverageNusselt number.
P	Pressure, [N/m^2].
P^*	Nondimensionalpressure, $\left(P - P_0\right) / \rho_0 V_0^2$.
Pr	Prandtl number, (ν/α).
r^*	Nondimensional radial coordinate.
Re	Reynolds number, $\left(V_0 D_h / \nu_0\right)$.
Ri	Richardson number, *(Gr/Re^2)*.
t^*	Nondimensional time, $\left(V_0 t / D_h\right)$.
T^*	NondimensionalTempérature, $\left(T - T_0\right) / \left(G\ D_h^2 / K_s\right)$.
V_0	Axialmean velocity at the entrance, [m/s].
V_θ^*	Nondimensional circumferential velocity component, $\left(V_\theta / V_0\right)$.
V_r^*	Nondimensional radial velocity component, $\left(V_r / V_0\right)$.
V_z^*	Nondimensional axial Velocity component, $\left(V_z / V_0\right)$.
z^*	Nondimensional axial coordinate, $\left(z / D_h\right)$.

Greek symbols

α	Thermal diffusivity, [m^2 ·s^{-1}]
β	Thermal expansion coefficient, [K^{-1}]
ε	Emissivity coefficient
μ	Dynamic viscosity, [kg·m·s^{-1}]
μ^*	Non-dimensional dynamic viscosity ($=\mu/\mu_0$)
ν	Kinematic viscosity, [m^2·s^{-1}]
θ	Angular coordinate, [rad]
ρ	Density, [kg m^{-3}]
σ	Stephan-Boltzmann constant (= 5.67· 10^{-8}),

$[W \cdot m^{-2} \cdot K^{-4}]$

τ Stress, $[N \cdot m^{-2}]$

τ^* Non-dimensional stress $(= \tau / (\mu_0 V_0 / D_i))$

II. INTRODUCTION

Laminar mixed convection between two concentric pipes has been studied by several workers. Nguyen et al. [1], studied theoretically the water flow in a concentric annulus, the surfaces of the system are considered is other mal and the pressure gradient along the annulus is constant. Thegoverningsystem of equationsis solved by thefinite difference method.The results areobtained from awater temperaturebetween0and150°C, this temperature range corresponds to a Prandtl number between 1 and 14. The author shaves shown that the axial flow is influenced by the natural convection, thereby changing theaxisymmetricshapeof the velocity fieldand temperature. The effect of the Prandtl number of the axia flow is presented for the case of Ra=104andaradius ratio Re/Ri =2. The obtained results show that the increasing of the Prandtl number make the axial velocity fields close to that of the forced convection. A good agreement is obtained with existing experimental and numerical results. Kotake et al [2], studied numerically the same problem, two different boundary conditions: a constant heat flux, constant temperature of the outer wall. The numerical results of average Nusselt number is in good agreement with other experimental results.Similar works has been done numerically by Kumar [3], and Chung et al. [4], Nouar [5], where the ratioD_O/D_Iwasconsidered. In the work ofHabib et al [6], the inner cylinder subjected to a non-uniform heat flux, while the outer surface is adiabatic, the change in axial Nusselt number in this work is in good agreement that of a numerical study under the same condition.

Experimentally,the heat transferbymixed convectioninannuluswas studied byMohammed et al [7], the two concentric cylindersare made of steel, $D_O/D_I = 2$,the inner tubesubjected toconstant heat flux,theouter tubeis adiabatic, the Reynolds numberisvariedfrom 200 to 1000, while the Grashofnumber variationisbetween $6.2 \cdot 10^5$ and $1.2 \cdot 10^7$, the results show that theaverageNusselt numbercan be linkedwithdifferentdimensionless numbersby the correlation:

$$Nu_m = 2.964(\mathrm{Gr} \cdot \mathrm{Pr}/\mathrm{Re})^{0.0326}$$

In this work, we studied numerically the heat transfer by mixed convection in an annulus between two concentric cylinders, the physical properties of the fluid are thermo-dependent and the heat losses with the external environment are considered. The objective of our study is the correlation of average Nusselt numbers and Richardson.

III. THE GEOMETRY AND MATHEMATICAL MODEL

Fig.1 illustrates the problem geometry. We consider a long two horizontal concentric pipes having a length L = 1 m. The internal pipe with an inside diameter D_{1i} = 0.96 cm and an external diameter D_{1o} = 1 cm, the external pipe with an inside diameter D_{2i} = 2 cm and an external diameter D_{2o} = 2.04 cm. The hydraulic diameter $D_h = D_{2i} - D_{1o}$ = 1 cm. The pipes are made of Inconel having a thermal conductivity K_s = 20W/m°K.

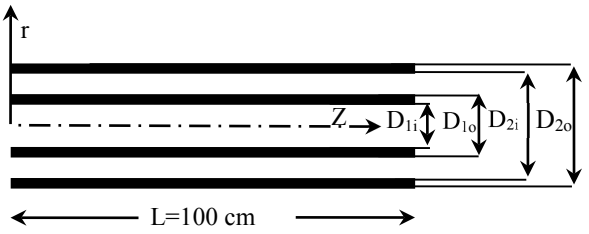

Fig. 1 Geometry of the Problem

The passing of an electrical intensity along the thickness of external pipe produced a generation of heat by the Joule effect, the consideredelectrical intensity values are: I =40, 45, 50, 55, 60 and 65 Amperes. This heat is transferred to laminar incompressible flow of distilled waterwith an average velocity equal to 5.69 10^{-2} m/s in the annulus.The inside surface of internal pipe is insulated, at the outer surface of external pipe, the heat losses by radiationand natural convection to the surrounding air are taken into account. At the annulus entrance, we have a uniform temperature equal to 288K, the Reynolds number Re is equal to 500, the Prandtl number Pris equal to 8.082 and the Grashof numbers Grcorrespond to the electrical intensities are:55734, 70538, 87084, 105372, 125401, and 147173, respectively. The non-dimensional fluid viscosity and thermal conductivity variation with temperature are represented by the functions $\mu^*(T^*)$ and $K^*(T^*)$ obtained by smooth fittings of the tabulated values cited by Baehr and Stephan [8]. The combined heat transfer in the solid and fluid domains is a conjugate heat transfer problem. The physical principles involved in this problem are well modelled by the following non dimensional conservation partial differential equations with their initial and boundary conditions:

A. Modelling Equations

$$\text{At } t^* = 0, \quad V_r^* = V_\theta^* = V_z^* = T^* = 0 \tag{1}$$

At $t^* > 0$,

1) Mass Conservation Equation

$$\frac{1}{r^*}\frac{\partial}{\partial r^*}\left(r^* V_r^*\right) + \frac{1}{r^*}\frac{\partial V_\theta^*}{\partial \theta} + \frac{\partial V_z^*}{\partial z^*} = 0 \tag{2}$$

2) Radial Momentum Conservation Equation

$$\frac{\partial V_r^*}{\partial t^*} + \frac{1}{r^*}\frac{\partial}{\partial r^*}\left(r^* V_r^* V_r^*\right) + \frac{1}{r^*}\frac{\partial}{\partial \theta}\left(V_\theta^* V_r^*\right) + \frac{\partial}{\partial z^*}\left(V_z^* V_r^*\right) - \frac{V_\theta^{*2}}{r^*} = -\frac{\partial P^*}{\partial r^*} + \frac{Gr_0^*}{\mathrm{Re}_0^2}\cos\theta\ T^* + \frac{1}{\mathrm{Re}_0}\left[\frac{1}{r^*}\frac{\partial}{\partial r^*}\left(r^* \tau_{rr}^*\right) + \frac{1}{r^*}\frac{\partial}{\partial \theta}\left(\tau_{r\theta}^*\right) - \frac{\tau_{\theta\theta}^*}{r^*} + \frac{\partial}{\partial z^*}\left(\tau_{rz}^*\right)\right] \tag{3}$$

3) Angular Momentum Conservation Equation

$$\frac{\partial V_\theta^*}{\partial t^*}+\frac{1}{r^*}\frac{\partial}{\partial r^*}\left(r^* V_r^* V_\theta^*\right)+\frac{1}{r^*}\frac{\partial}{\partial \theta}\left(V_\theta^* V_\theta^*\right)+\frac{\partial}{\partial z^*}\left(V_z^* V_\theta^*\right)+\frac{V_r^* V_\theta^*}{r^*}=-\frac{1}{r^*}\frac{\partial P^*}{\partial \theta}-\frac{Gr_0^*}{\mathrm{Re}_0^2}\sin\theta\ T^*+\frac{1}{\mathrm{Re}_0}\left[\frac{1}{r^{*2}}\frac{\partial}{\partial r^*}\left(r^{*2}\tau_{\theta r}^*\right)+\frac{1}{r^*}\frac{\partial}{\partial \theta}\left(\tau_{\theta\theta}^*\right)+\frac{\partial}{\partial z^*}\left(\tau_{\theta z}^*\right)\right] \quad (4)$$

4) Axial Momentum Conservation Equation

$$\frac{\partial V_z^*}{\partial t^*}+\frac{1}{r^*}\frac{\partial}{\partial r^*}\left(r^* V_r^* V_z^*\right)+\frac{1}{r^*}\frac{\partial}{\partial \theta}\left(V_\theta^* V_z^*\right)+\frac{\partial}{\partial z^*}\left(V_z^* V_z^*\right)=-\frac{\partial P^*}{\partial z^*}+\frac{1}{\mathrm{Re}_0}\left[\frac{1}{r^*}\frac{\partial}{\partial r^*}\left(r^*\tau_{rz}^*\right)+\frac{1}{r^*}\frac{\partial}{\partial \theta}\left(\tau_{\theta z}^*\right)+\frac{\partial}{\partial z^*}\left(\tau_{zz}^*\right)\right] \quad (5)$$

5) Energy Conservation Equation

$$\frac{\partial T^*}{\partial t^*}+\frac{1}{r^*}\frac{\partial}{\partial r^*}\left(r^* V_r^* T^*\right)+\frac{1}{r^*}\frac{\partial}{\partial \theta}\left(V_\theta^* T^*\right)+\frac{\partial}{\partial z^*}\left(V_z^* T^*\right)=G^*-\frac{1}{\mathrm{Re}_0\ \mathrm{Pr}_0}\left[\frac{1}{r^*}\frac{\partial}{\partial r^*}\left(r^* q_r^*\right)+\frac{1}{r^*}\frac{\partial}{\partial \theta}\left(q_\theta^*\right)+\frac{\partial}{\partial z^*}\left(q_z^*\right)\right] \quad (6)$$

Where $G^*=\begin{cases}K_S^*/\left(\mathrm{Re}_0\ \mathrm{Pr}_0\right) & in\ \ the\ \ solid\\ 0 & in\ \ the\ \ fluid\end{cases}$

The viscous stress tensor components are:

$$\tau_{rr}^*=2\mu^*\frac{\partial V_r^*}{\partial r^*},\quad \tau_{r\theta}^*=\tau_{\theta r}^*=\mu^*\left[r^*\frac{\partial}{\partial r^*}\left(\frac{V_\theta^*}{r^*}\right)+\frac{1}{r^*}\frac{\partial V_r^*}{\partial \theta}\right]$$

$$\tau_{\theta\theta}^*=2\mu^*\left[\frac{1}{r^*}\frac{\partial V_\theta^*}{\partial \theta}+\frac{V_r^*}{r^*}\right],\quad \tau_{\theta z}^*=\tau_{z\theta}^*=\mu^*\left[\frac{\partial V_\theta^*}{\partial z^*}+\frac{1}{r^*}\frac{\partial V_z^*}{\partial \theta}\right] \quad (7)$$

$$\tau_{zz}^*=2\mu^*\frac{\partial V_z^*}{\partial z^*},\quad \tau_{zr}^*=\tau_{rz}^*=\mu^*\left[\frac{\partial V_z^*}{\partial r^*}+\frac{1}{r^*}\frac{\partial V_r^*}{\partial z^*}\right]$$

The heat fluxes are:

$$q_r^*=-K^*\frac{\partial T^*}{\partial r^*},\quad q_\theta^*=-\frac{K^*}{r^*}\frac{\partial T^*}{\partial \theta^*}\ \ and\ \ q_Z^*=-K^*\frac{\partial T^*}{\partial z^*} \quad (8)$$

B. The Boundary Conditions

1) At the Annulus Entrance : $Z^*=0$

**In the Fluid Domain:* $0.5435 \le r^* \le 1.0435$ *and* $0 \le \theta \le 2\pi$

$$V_r^*=V_\theta^*=T^*=0,\ V_z^*=1 \quad (9)$$

**In the Solid Domain:*

$0.5 \le r^* \le 0.5435$ *or* $1.0435 \le r^* \le 1.0870$ *and* $0 \le \theta \le 2\pi$

$$V_r^*=V_\theta^*=V_z^*=T^*=0 \quad (10)$$

2) At the Annulus Exit : $Z^*=217.39$

**In the Fluid Domain:* $0.5435 \le r^* \le 1.0435$ *and* $0 \le \theta \le 2\pi$

$$\frac{\partial V_r^*}{\partial z^*}=\frac{\partial V_\theta^*}{\partial z^*}=\frac{\partial V_z^*}{\partial z^*}=\frac{\partial}{\partial z^*}\left(K^*\frac{\partial T^*}{\partial z^*}\right)=0 \quad (11)$$

**In the Solid Domain:*

$0.5 \le r^* \le 0.5435$ *or* $1.0435 \le r^* \le 1.0870$ *and* $0 \le \theta \le 2\pi$

$$V_r^*=V_\theta^*=V_z^*=\frac{\partial}{\partial z^*}\left(K^*\frac{\partial T^*}{\partial z^*}\right)=0 \quad (12)$$

3) At the Inside Wall of Internal Pipe: $r^*=0.5$

$$V_r^*=V_\theta^*=V_z^*=0\ \ and\ \ \frac{\partial T^*}{\partial r^*}=0 \quad (13)$$

4) At the Outer Wall of External Pipe: $r^*=1.0870$

$$\begin{cases}V_r^*=V_\theta^*=V_z^*=0\\ -K^*\dfrac{\partial T^*}{\partial r^*}=\dfrac{(h_r+h_c)D_i}{K_0}T^*\end{cases} \quad (14)$$

$$h_r=\varepsilon\sigma\left(T^2+T_\infty^2\right)\left(T+T_\infty\right) \quad (15)$$

The emissivity of the outer wall ε is arbitrarily chosen to 0.9 while h_c is derived from the correlation of Churchill and Chu [9] valid for all Pr and for Rayleigh numbers in the range $10^{-6} \le \mathrm{Ra} \le 10^9$.

$$Nu=\left[h_c\ D_i/K_{air}\right]=\left[0.6+\left(0.387\ Ra^{1/6}/\left(1+\left(0.559/\mathrm{Pr}_{air}\right)^{9/16}\right)^{8/27}\right)\right]^2 \quad (16)$$

C. Nusselt Number

At the solid-fluid interface ($r^*=1.0435$) the local Nusselt number is defined as:

$$Nu\ (\theta,Z^*)=\frac{h(\theta,Z^*)D}{k}=\frac{1}{\left[T^*(r^*,\ \theta,\ z^*)-T_m^*(z^*)\right]} \quad (17)$$

The axial Nusselt number is defined as:

$$Nu\ (z^*)=\frac{1}{2\pi}\int_0^{2\pi} Nu\ (\theta,z^*)\,d\theta \quad (18)$$

The average Nusselt number for the whole solid-fluid interface is defined as:

$$Nu_A=\frac{1}{(2\pi)\ (217.39)}\int_0^{2\pi}\int_0^{217.39} Nu(\theta,z^*)\ dz^*\ d\theta \quad (19)$$

IV. THE NUMERICAL METHOD

For the numerical solution of modelling equations, we used the finite volume method well described by Patankar [10]. The using of this method involves the discretization of the physical domain into a discrete domain constituted of finite volumes where the modelling equations are discretized in a typical volume. We used a temporal discretization with a truncation error of $\left(\Delta t^*\right)^2$ order. The mesh used contains 26×44×162 points in the radial, azimuthal and axial directions. The considered time step is $\Delta t^*=5\cdot10^{-4}$. The

accuracy of the results of our numerical code has been tested by the comparison of our results with those of Nouar[11] who studied numerically the effect of the dynamic viscosity of the mixed convection between two concentric horizontal pipes.The inner cylinderand the outer cylinderaresubjected to aconstant heat flux The controlling parameters of the problem are: Re = 35, Pr= 557.3, Gr = 6000, $L/D_h = 125$. In Fig. 2we illustrate the axial temperature variation at the top (θ =0) and bottom (θ =π) oftheexternalinterface (fluid-outer pipe).

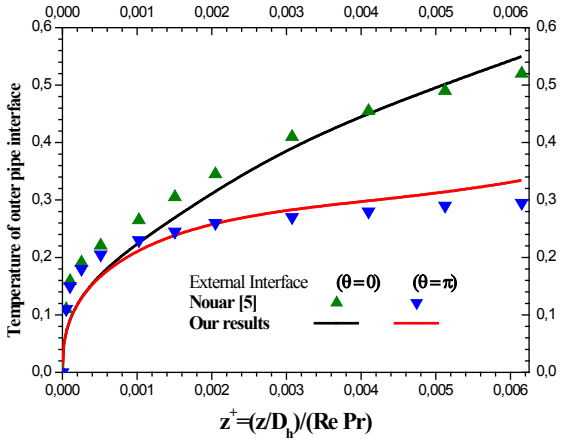

Fig. 2 Axial Evolution of the interface temperature (fluid-Outer pipe); a Comparison with theResults of Nouar[5].

It is seen that there is a good agreement between our results and theirs.

V. RESULTS AND DISCUSSIONS

A. Development of the Secondary Flow

The obtained flowfor theconsidered cases is characterized byamain flowin the axial directionandasecondary flowin (r^*, θ) plan.Qualitativelywe note thesimilarity of resultsfor the sixstudy cases.Quantitatively,the effect ofmixed convectionbecomesincreasinglyimportantwith the increase ofvolumetricheating. For this, the figures presented are those of the higher volumetric heating, case of Gr = 147173. In fig. 3, we present the secondary flow at the annulus exit (Z^*=100). Thetransverse movementis explained as follows: the hot fluid moves along the hot wall from the bottom of the outer tube (θ=π)upwards(θ=0)and moves down from the top to the bottom along the inner tube. The vertical plane passing through the angles (θ=0)and (θ=π) is a plane of symmetry.

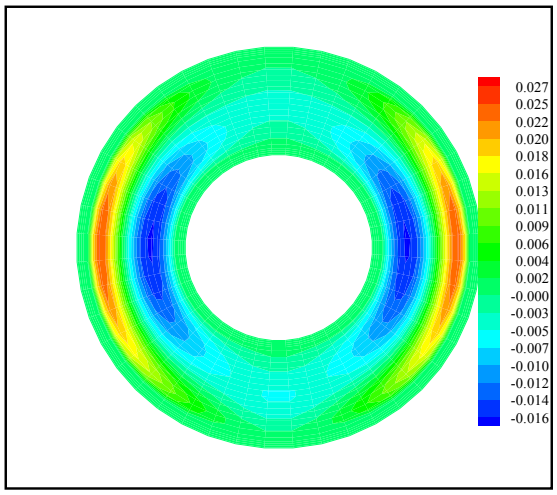

Fig. 3 Secondary Flow at the Exit of the Annulus for Gr=147173

The transverse flow in the (r^*, θ) plane is represented by two similar but counter rotating cells. We noticed that the centre of the rotating cells moves downward continuously along the axial direction.

B. Development of the Axial Flow

At the entrance, the axial flow is axisymmetric, after this latter is influenced by the transverse movement of the fluid. The maximum axial velocity is all the time at the top of the annulus because the fluid viscosity decreased from bottom to top. In fig.4, we present the axial flow distribution at the exit of the annulus.

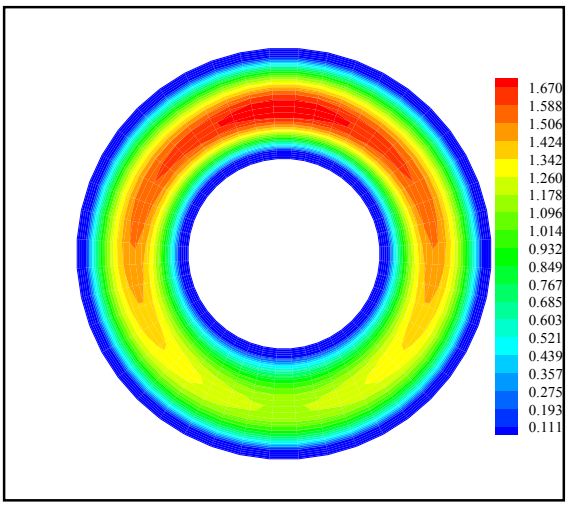

Fig. 4 Axial Velocity Profiles at the Exit of the Annulus for Gr=147173

C. Development of the Temperature Field

In the reference case(forced convection), the distribution of the fluid temperature in the absence of transverse motion is axisymmetric. For a given section, the isotherms are concentric circles with a maximum temperature on the inner wall of the external cylinder and a minimum temperature on the outer wall of the internal cylinder. In the presence of volumetric heating, a transverse flow exists and thus changes

the axisymmetric distribution of fluid and pipe wall temperature and gives it an angular variation, this variation explained as follows: the hot fluid near the hot pipe wall moves upwards under the buoyancy force effect, the relatively cold fluid descends down near the internal pipe.This movement of the secondary flow is the cause of the azimuthally temperature variation.The obtained results show that at given section, the maximum temperature T^* is all the time located at r^*=1 and θ=0 (top of solid-fluid interface), because the hot fluid is driven by the secondary motion towards the top of the annulus.The minimum temperature is within the core fluid, in the lower part of the annulus at θ=π. In fig. 5, we present the polar temperature distribution at the exit of the annulus for *Gr*=147173.

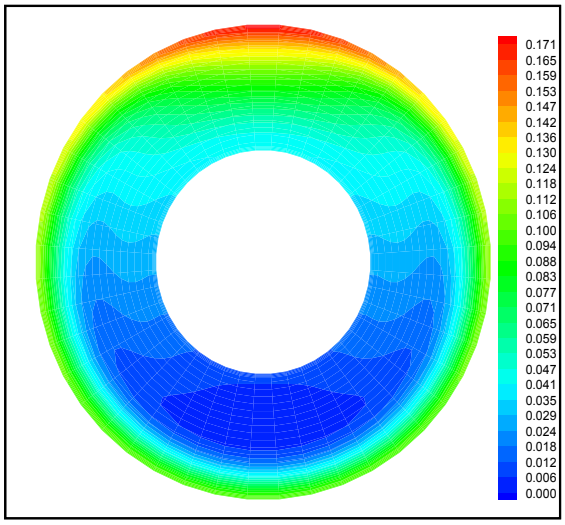

Fig. 5 The Isotherms at the Exit of the Annulus for Gr=147173

D. The Nusselt numbers

The phenomenon of heat transfer has been characterised in terms of circumferentially Nusselt numbers calculated at the inner wall of external pipe, which is obtained by (19). The variation of local Nusselt number of the solid-fluid interface is presented in fig. 8 for Gr=147173.From the entrance to the exit, we notice the large axial and angular variations of local Nusselt numbers, it takes a minimum value at (θ=0) and maximum value at(θ=π).

Fig. 9 shows the axial variation of Nusselt number for the seven studied cases. At the zone of entrance, the axial Nusselt number decreases rapidly for all studied cases. After, it increases and takes maximum value at the exit of annulus equal to: 7.58, 7.96, 8.35, 8.74, 9.06 and 9.45 for *Gr* = 55734, 70538, 87084, 105372, 125401, and 147173respectively. The axial Nusselt numbers increases with the increase of volumetric heating.

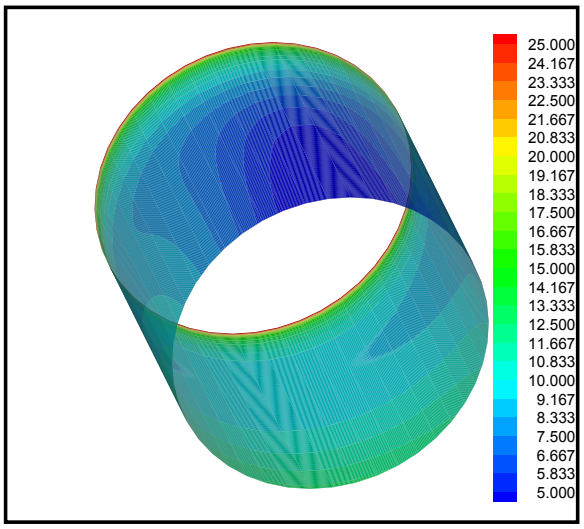

Fig. 8 The Local Nusselt Number Variation for Gr =147173.

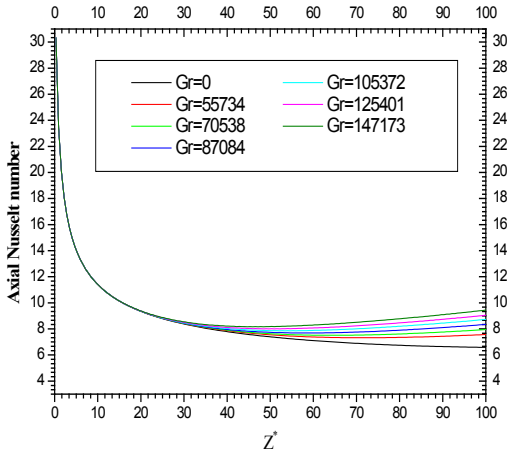

Fig. 9 Nusselt Number Variation for Different Grashof Numbers

In Tab. 1 we present the average Nusselt numbers of all studied cases:

TABLE I. Average Nusselt Numbers

Gr	55734	70538	87084	105372	125401	147173
Ri	0.223	0.282	0.348	0.421	0.502	0.589
Nu_A	8.803	8.928	9.068	9.220	9.359	9.529

The results obtained allowed us to model the average Nusselt number of the mixed convection in function of Richardson number, we found that the results with the parameters used are correlated with the correlation:

$$Nu_A = 9.9130\ Ri^{0.0816} \quad (22)$$

VI. CONCLUSION

This study considers the numerical simulation of the three dimensional mixed convection heat transfer in horizontal annulus, the external pipe is heated by an electrical intensity passing through its small thickness and the internal pipe is insulated.The obtained results show that:

* The dynamic and thermal fields for mixed convection are qualitatively and quantitatively different from those of forced convection.

* Although the volumetric heat input in the solid thickness is constant, the heat flux at the solid-fluid interface is not constant: it varies with θ and z, that is a characteristic of the considered mixed convection.

* The azimuthally variation of temperature at a given section is important; this phenomenon is demonstrated by the circumferential temperature variation of the wall. There is a large temperature wall difference between top and bottom of the external pipe.

* The physical properties are thermo-dependent (the dimensionless dynamic viscosity varies from 1.018 at the entrance to 0.4171 at the exit).

* For the forced convection, the average Nusselt number is 8.803. Thus, for the mixed convection, the parameters used are well correlated with the correlation:$NU_A = 9.9130\ RI^{0.0816}$.

VII. REFERENCES

[1] T.H. Nguyen, P. Vasseur, L. Robillard, B. Shekhar, “Combined free and forced convection of water between horizontal concentric annuli*”, J. Heat Transfer*, Vol. 105, 1983, pp.498-504.

[2] S. Kotake, N. Hattori, "Combined forced and free convection heat transfer for fully-developed laminar flow in horizontal annuli", *Int. J. Heat Mass Transfer*, vol. 28, 1985, pp. 2113-2120.

[3] R. Kumar, "Study of natural convection in horizontal annuli", *Int. J. Heat Mass Transfer*, vol. 31, 1988, pp. 1137-1148.

[4] S. Y. Chung, G. H. Rhee, et H. J. Sung, "Direct Numerical Simulation of Concentric Annular Pipe Flow"*Part I: Flow Field, Int. J. Heat Fluid Flow*, vol. 23, 2002, pp. 426-440.

[5] C. NOUAR, "Numerical solution for laminar mixed convection in a horizontal annular duct: temperature-dependent viscosity effect", *Int. J. Numer. Meth. Fluids* Vol. 29, 1999, pp. 849–864.

[6] M. A. Habib, A. A. A. Negm, "Laminar mixed convection in horizontal concentric annuli with non-uniform circumferential heating" , *Int. J. Heat Fluid Flow*, Vol. 37, 2001, pp. 427-435.

[7] H.A. Mohammed, Antonio Campo, R. Saidur, "Experimental study of forced and free convective heat transfer in the thermal entry region of horizontal concentric annuli", *International Communications in Heat and Mass Transfer*, Vol. 37, 2010, pp. 739–747.

[8] H.D. Baehr and K. Stephan, *Heat and Mass Transfer,* Transl, by N. JanePark, p. 619, pringer-Verlag, Berlin: 1998.

[9] S.W. Churchill, H.S. Chu, "Correlating Equation for Laminar and Turbulent Free Convection from a Horizontal Cylinder", *International Journal of Heat and Mass Transfer,* Vol 18, 1975, pp. 1049-1053

[10] S.V. Patankar, *Numerical Heat Transfer and Fluid Flow*, McGraw-Hill, New-York: 1980.

MINERALOGICAL CHARACTERIZATION OF SANDSTONE AND CLAY, NORTH-EAST CONSTANTINE.

Submited on 08/03/2014 – Accepted on 19/12/2015

Abstract

The north-east area of Constantine has a very complex geological setting. The variety of sedimentary rocks such as sandstone and clay in abundance, represent a big importance in the industry and road infrastructure.
The X-ray diffraction (XRD) analysis, Scanning Electron Microscopy SEM/EDS, FTIR spectroscopy of sandstone and clay are required for qualitative and quantitative analysis of the existing phases.
In addition, chemical analysis of the same samples is required to confirm the XRD, EDS (Energy Dispersive X ray Spectroscopy) and FTIR spectroscopy results.
The results of this multidisciplinary study, obtained by various analytical techniques, show a good agreement on the existing phases.

Keywords: *Sandstone, Clay, XRD, SEM/EDS, FTIR*

M BENYAMINA
L CHETIBI
M BOUCHEAR

Materials Sciences and Applications Research Unit, Department of Physics, Faculty of Exact Sciences, Frères Mentouri University, Constantine, Algeria.

NOMENCLATURE

a	Defined constant in the elliptic coordinates, (distance to the poles).	(m)
c_p	Specific heat at constant pressure.	($J.kg^{-1}.K^{-1}$)
e_1	Eccentricity of the internal ellipse.	
Fr	Geometrical factor of form	
$\vec{g}$	Gravitational acceleration.	($m.s^{-2}$)
Gr	Grashof number defined by $Gr = \frac{g\beta a^3}{\upsilon^2}\Delta T$.	
h	Dimensional metric coefficient.	(m)
H	Dimensionless metric coefficient.	
Nu	Local Nusselt number.	
$\overline{Nu}$	Average Nusselt number.	
P	Stress tensor.	
Pr	Prandtl number defined by $\Pr = \frac{\nu \rho c_p}{\lambda}$.	
S_Φ	Source term.	
T	Fluid's temperature.	(K)
T_1	Hot wall temperature.	(K)
T_2	Cold wall temperature.	(K)
ΔT	Temperature deference.$\Delta T=T_1-T_2$.	(K)
V_η, V_θ	Velocity components according to η and θ.	($m.s^{-1}$)
$\vec{V}$	Velocity vector.	($m.s^{-1}$)

Greek letters

α	Inclination angle.	(°)
β	Thermal expansion coefficient.	(K^{-1})
Γ_φ	Diffusion coefficient.	
λ	Thermal conductivity of the fluid.	($W.m^{-1}.K^{-1}$)
υ	kinematic viscosity.	($m^2.s^{-1}$)
ρ	Density.	($kg.m^{-3}$)
η ,θ, z	Elliptic coordinates.	
ψ	function of current.	($m^2.s^{-1}$)
ω	vorticity.	(s^{-1})
φ	General function.	

Superscripts

+	dimensionless parameters.

Subscripts

i	Inner.
e	Outer.
éq	Equivalent
Ni	Points number along the coordinate η
NN	Points number along the coordinate θ
η	According to the coordinate η
θ	According to the coordinate θ

1. INTRODUCTION

The study of heat transfer by natural convection, in the annular spaces formed by elliptic cylinders with horizontal axes centered or eccentric, has given rise to many works include such as Zhu et al. (2004) who have made a numerical study into the annulus between two centered elliptic cylinders, using D.Q method (Differential Quadrature) to solve their equations. Djezzar el al. (2004), (2005) and (2006) mean while, have studied numerically natural convection in an annulus formed by two elliptical cylinders and horizontal axes confocal using the formulation in primitive variables, they could detect multi-cellular flows when Grashof number increases, for certain geometries, and for the three parietal thermal conditions used.

In this work we propose a numerical simulation using the finite-volume method described by Patankar (1980), the elliptic coordinates cited by Moon (1961) and the vorticity stream-function formulation illustrated by Nogotov (1978) to solve the equations governing the phenomenon studied. The mesh adopted for the execution of our calculations is (101x111).

2. Theoretical analysis

We consider an annular space, filled with a Newtonian fluid (in this case air), located between two elliptical cylinders, and two horizontal and centered diametrical planes. Figure 1 represents a cross-section of the system.

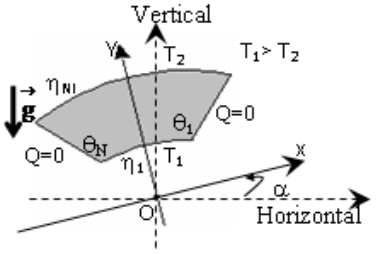

FIG. 1 Cross-section of the system

Both lower and upper walls are elliptical, isothermal and respectively maintained at temperatures T_1 and T_2 with $T_1>T_2$. The two diametrical plans are adiabatic.

It occurs in the enclosure natural convection that we propose to study numerically.

We consider an incompressible fluid flow, two dimensional, permanent and laminar with constant physical properties and we use the approximation of Boussinesq which considers the variations of the density ρ negligible at all terms of the momentum equations except in the term of gravity whose variations with temperature supposed linear, generate the natural convection.

Viscous dissipation and the work of pressure forces are negligible in the heat equation; the radiation is not considered.

With these assumptions the equations governing our problem can be written in vectorial form as follows:

- Continuity equation:

$$\mathrm{div}\,\vec{V} = 0 \tag{1}$$

- Momentum equation:

$$(\vec{V}.\vec{\mathrm{grad}})\vec{V} = \frac{\rho}{\rho_0}\vec{g} + \frac{\nabla P}{\rho_0} \tag{2}$$

- Heat equation:

$$(\vec{V}.\vec{\mathrm{grad}})T = \frac{\lambda}{\rho c_p}\nabla^2 T \tag{3}$$

It is convenient to define a reference frame such as the limits of the system result in constant values of the coordinates. The coordinates known as "elliptic" (η,θ) allow, precisely in our case to obtain this result. Thus the two elliptic isothermal walls will be represented by η_1 and η_{NI} and the two adiabatic walls will be represented by θ_1 and θ_{NN}. The transition from Cartesian coordinates to elliptic coordinates is done using the following relations:

$$\left.\begin{aligned} x &= a.ch(\eta).\cos(\theta) \\ y &= a.sh(\eta).\sin(\theta) \end{aligned}\right\}$$

The equations (1), (2) and (3) are written respectively:

$$\frac{\partial}{\partial\eta}(h V_\eta) + \frac{\partial}{\partial\theta}(h V_\theta) = 0 \tag{5}$$

$$\frac{V_\eta}{h}\frac{\partial\omega}{\partial\eta} + \frac{V_\theta}{h}\frac{\partial\omega}{\partial\theta} =$$

$$\frac{g\beta}{h}\left\{\begin{aligned} &[F(\eta,\theta)\cos(\alpha) - G(\eta,\theta)\sin(\alpha)]\frac{\partial T}{\partial\eta} \\ &-[F(\eta,\theta)\sin(\alpha) + G(\eta,\theta)\cos(\alpha) +]\frac{\partial T}{\partial\theta} \end{aligned}\right\}$$

$$+\frac{\nu}{h^2}\left(\frac{\partial^2\omega}{\partial\eta^2} + \frac{\partial^2\omega}{\partial\theta^2}\right) \tag{6}$$

$$V_\eta\frac{\partial T}{\partial\eta} + V_\theta\frac{\partial T}{\partial\theta} = \frac{\lambda}{\rho c_p}\frac{1}{h}\left(\frac{\partial^2 T}{\partial\eta^2} + \frac{\partial^2 T}{\partial\theta^2}\right) \tag{7}$$

With the introduction of vorticity defined by:

$$\omega = -\frac{1}{h^2}\left(\frac{\partial^2\psi}{\partial\eta^2} + \frac{\partial^2\psi}{\partial\theta^2}\right) \tag{8}$$

After the introduction of the stream-function, in order to check the continuity equation identically.

$$\left.\begin{aligned} h &= a\left(sh^2(\eta) + \sin^2(\theta)\right)^{1/2} \\ F(\eta,\theta) &= \frac{sh(\eta)\cos(\theta)}{\left(sh^2(\eta) + \sin^2(\theta)\right)^{1/2}} \\ G(\eta,\theta) &= \frac{ch(\eta)\sin(\theta)}{\left(sh^2(\eta) + \sin^2(\theta)\right)^{1/2}} \end{aligned}\right\} \tag{9}$$

By posing the following adimensional quantities:

D_h= a (arbitrarily selected focal distance)

$$H = \frac{h}{D_h},\quad V_\eta^+ = V_\eta\frac{D_h}{\nu},\quad V_\theta^+ = V_\theta\frac{D_h}{\nu},\quad \omega^+ = \omega\frac{D_h^2}{\nu},$$
$$\psi^+ = \frac{\psi}{\nu} \text{ and } T^+ = \frac{T - T_2}{T_1 - T_2}$$

The equations (5), (6), (7) and (8) becomes:

$$\frac{\partial}{\partial\eta}(H V_\eta^+) + \frac{\partial}{\partial\theta}(H V_\theta^+) = 0 \tag{10}$$

$$\frac{V_\eta^+}{H}\frac{\partial \omega^+}{\partial \eta}+\frac{V_\theta^+}{H}\frac{\partial \omega^+}{\partial \theta}=$$

$$\frac{Gr}{H}\left\{\begin{array}{l}\left[F(\eta,\theta)\cos(\alpha)-G(\eta,\theta)\sin(\alpha)\right]\frac{\partial T^+}{\partial \eta}\\ -\left[\mathrm{F}(\eta,\theta)\sin(\alpha)+G(\eta,\theta)\cos(\alpha)+\right]\frac{\partial T^+}{\partial \theta}\end{array}\right\}$$

$$+\frac{1}{\mathrm{H}^2}\left(\frac{\partial^2 \omega^+}{\partial \eta^2}+\frac{\partial^2 \omega^+}{\partial \theta^2}\right) \qquad (11)$$

$$HV_\eta^+\frac{\partial \mathrm{T}^+}{\partial \eta}+\mathrm{H}V_\theta^+\frac{\partial \mathrm{T}^+}{\partial \theta}=\frac{1}{\mathrm{P_r}}\left(\frac{\partial^2 \mathrm{T}^+}{\partial \eta^2}+\frac{\partial^2 \mathrm{T}^+}{\partial \theta^2}\right) \qquad (12)$$

$$\omega^+=-\frac{1}{H^2}\left[\frac{\partial^2 \psi^+}{\partial \eta^2}+\frac{\partial^2 \psi^+}{\partial \theta^2}\right] \qquad (13)$$

The boundary conditions are: For the elliptical hot wall ($\eta = \eta_1$= constant) we have:

$V_\eta^+ = V_\theta^+ = \frac{\partial \psi^+}{\partial \theta} = \frac{\partial \psi^+}{\partial \eta} = 0$, $T_1^+ = 1$ and

$\omega^+=-\frac{1}{H^2}\left[\frac{\partial^2 \psi^+}{\partial \eta^2}+\frac{\partial^2 \psi^+}{\partial \theta^2}\right]$ and for the cold elliptic wall ($\eta=\eta_{NN}$=constant) we have:

$V_\eta^+ = V_\theta^+ = \frac{\partial \psi^+}{\partial \theta} = \frac{\partial \psi^+}{\partial \eta} = 0$, $T_2^+ = 0$ and

$\omega^+=-\frac{1}{H^2}\left[\frac{\partial^2 \psi^+}{\partial \eta^2}+\frac{\partial^2 \psi^+}{\partial \theta^2}\right]$. For the two diametrical plans ($\theta = \theta_1$= constant and $\theta = \theta_{NN}$=constant) we have:

$V_\eta^+ = V_\theta^+ = \frac{\partial \psi^+}{\partial \theta} = \frac{\partial \psi^+}{\partial \eta} = 0$, $\frac{\partial T^+}{\partial \theta} = 0$ and

$$\omega^+=-\frac{1}{H^2}\left[\frac{\partial^2 \psi^+}{\partial \eta^2}+\frac{\partial^2 \psi^+}{\partial \theta^2}\right]$$

Once the temperature distribution is obtained; local Nusselt number value is given by the following relation:

$$Nu=-\frac{1}{H}\frac{\partial T^+}{\partial \eta}\bigg|_{\eta=cste} \qquad (14)$$

The average Nusselt number is expressed by:

$$\overline{Nu}=\frac{1}{\theta_{NN}-\theta_1}\int_{\theta_1}^{\theta_{NN}} Nu\,d\theta \qquad (15)$$

2. 1 Numerical Formulation

To solve the system of equations (11), (12) and boundary conditions, we consider a numerical solution by the finite volumes method. Where as for the equation (13), we consider a numerical solution by the centered differences method.

Both methods are widely used in the numerical solution of transfer problems; they are well exposed by Patankar (1980) and by Nogotov (1978). Figure 2 represents the physical and computational domain.

We cut out annular space according to the directions η and θ from the whole of elementary volumes or "control volume" equal to "$H^2.\Delta\eta.\Delta\theta.1$". (The problem is two-dimensional, the thickness in Z direction is assumed to the unity).

The center of a typical control volume is a point P and center of its side faces "east", "west", "north" and "south", are indicated respectively, by the letters e, w, n and s. Four other control volumes surround each interior control volume. The centers of these volumes are points E, W, N and S. the scalar variables (vorticity, temperature) are stored at centered points in control volumes. Thus transfer equations of scalar variables are integrated in typical control volume.

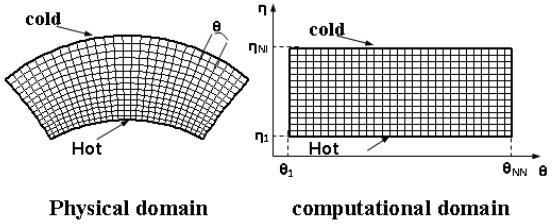

FIG. 2 Physical and computational domain

Figure 3 represents a typical control volume and its neighbors in a computational domain.

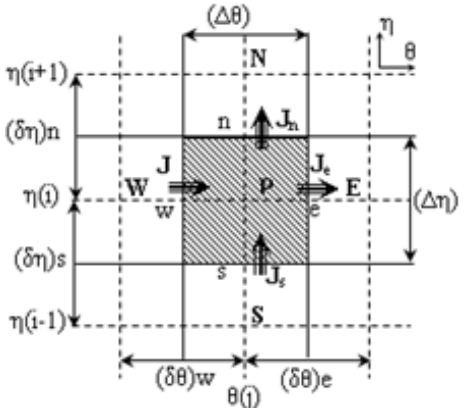

FIG. 3 A typical control volume and its neighbors in a computational domain

2. 2 Discretization of the general transfer equation of a variable φ in the control volume:

To illustrate the discretization of the transfer equations by finite volumes method, we consider the transfer equation in its general form:

$$\frac{\partial}{\partial \eta}\left(\mathrm{H}V_\eta^+\varphi-\Gamma_\varphi\frac{\partial \varphi}{\partial \eta}\right)+\frac{\partial}{\partial \theta}\left(\mathrm{H}V_\theta^+\varphi-\Gamma_\varphi\frac{\partial \varphi}{\partial \theta}\right)=S\varphi \qquad (16)$$

Sources and diffusion coefficients are specified in table 1.

Tab. 1 sources and diffusion coefficients of the variables φ

φ	Γ_φ	S_φ
T^+	1/Pr	0
ω^+	1	$\frac{Gr}{h}\left\{\begin{array}{l}[F(\eta,\theta)\cos(\alpha)-G(\eta,\theta)\sin(\alpha)]\frac{\partial T^+}{\partial \eta}\\ -[F(\eta,\theta)\sin(\alpha)+G(\eta,\theta)\cos(\alpha)]\frac{\partial T^+}{\partial \theta}\end{array}\right\}$

The discretization equation is obtained by integrating the conservation equations over the control volume shown in Figure 3 Patankar (1980), we obtain the following final form:

$$a_P \phi_P = a_N \phi_N + a_S \phi_S + a_E \phi_E + a_W \phi_W + b \qquad (17)$$

The coefficients of equation 17 are well defined by Patankar (1980), the Power Law scheme used to discretize the convectif terms in the governing equations.

3. RESULTS AND DISCUSSION

We consider two configurations for our cavity characterized by two values of inclination angle (0° and 45°) and a geometrical form factor (Fr = 5) which is defined by:

$$Fr = \frac{\eta_{NI} - \eta_1}{\theta_{NN} - \theta_1}$$

3.1 Grid study:

Several grids were used arbitrarily for the following configuration: (α=0° and Fr=1, for $Gr=10^3$, $Gr=10^4$ and $Gr=5.10^4$), to see their effect on the results, table 2 shows us the variation of average Nusselt number and the maximum of the stream function value according to the number of nodes for each grid. We choose the grid (101x111).

Tab. 2 Variation of average Nusselt number and the maximum of the stream-function value according to the number of nodes

	Gr =10^3		**Gr =10^4**		**Gr =5.10^4**	
$\eta_{NI}x\theta_{NN}$	ψ_{max}	$NU_{moy.}$	ψ_{max}	$NU_{moy.}$	ψ_{max}	$NU_{moy.}$
41x51	0.090	1.387	5.582	2.689	16.575	4.268
51x61	0.090	1.387	5.588	2.685	16.572	4.234
61x71	0.109	1.387	5.593	2.682	16.566	4.197
71x81	0.130	1.387	5.596	2.680	15.560	4.197
81x91	0.179	1.387	5.596	2.678	15.555	4.195
91x101	0.201	1.387	5.596	2.678	15.549	4.190
101x111	0.219	1.389	5.596	2.674	15.549	4.190
111x121	0.219	1.389	5.596	2.674	15.549	4.190

3.2 Numerical code validation

Kuehn et al. (1976) have developed a numerical study on natural convection in the annulus between two concentric and horizontal cylinders with a radius was taken equal to 2.6, they calculated a local equivalent thermal conductivity, defined as being the report of a temperature gradient in a convective and conductive heat exchange on a temperature gradient in an exchange conduction:

$$\lambda_{éq} = \frac{\left.\frac{\partial T^+}{\partial \eta}\right|_{convection+conduction}}{\left.\frac{\partial T^+}{\partial \eta}\right|_{conduction}}$$

They calculated an average value of the conductivity. To validate our numerical code, we compared the average value derived from our calculations with their results. Table 3 illustrates this comparison and we find that quantitatively our results and theirs are in good agreement.

Tab. 3 Comparison of the average thermal conductivity of Kuehn with our results

	Pr	0,70	0,70	0,70	0,70
	Ra	10^2	10^3	$6x10^3$	10^4
Inner wall	Kuehn	1,000	1,081	1,736	2,010
	Presents calculs	1,000	1,066	1,730	2,068
	|E(%)|	**0,000**	**1,388**	**0,346**	**2,886**
Outer wall	Kuehn	1,002	1,084	1,735	2,005
	Presents calculs	1,002	1,066	1,736	2,078
	|E(%)|	**0,000**	**1,661**	**0,058**	**3,641**

3.3 Influence of the Grashof number

3.4 Isotherms and streamlines

Figure 4 and figure 5 represent the isotherms and the streamlines for different values of the Grashof number when α=0°.

We note that these isotherms and these streamlines are symmetrical about the median fictitious vertical plane. These figures show that the structure of the flow is bi-cellular. The flow turns in the trigonometrically direction in the left side and in opposite direction in the right one (the fluid particles move upwards along the hot wall).

For $Gr=10^2$ the isotherms are almost parallel and concentric curves which coincide well with active walls profiles. In this case the temperature distribution is simply decreasing from the hot wall to the cold wall. The streamlines of the fluid show that the flow is organized in two cells that rotate very slowly in opposite directions.

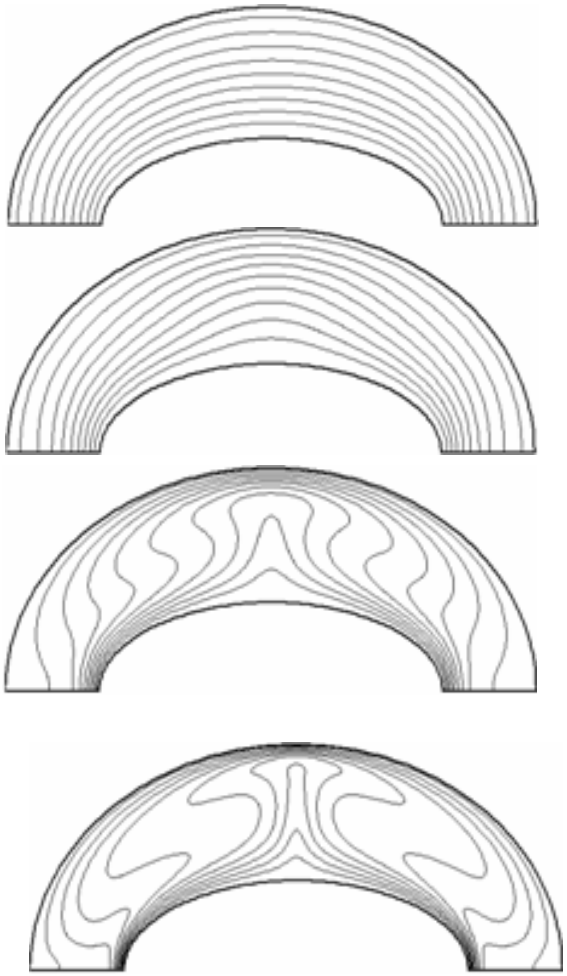

FIG. 4 Isotherms for e_1=0.86, Fr=5, α=0° and respectively Gr=10^2, Gr=10^3, Gr=10^4 and Gr=5.10^4

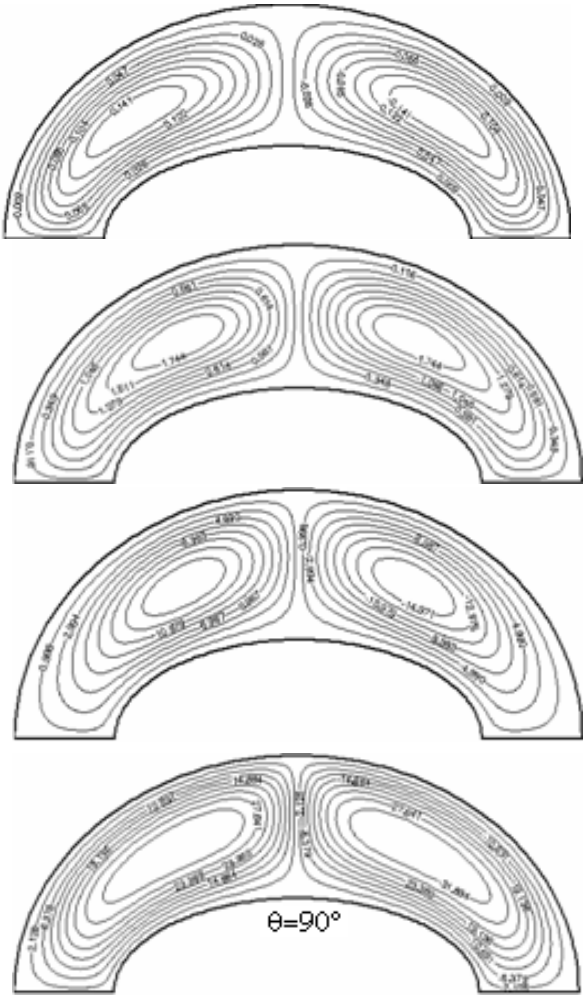

FIG. 5 Streamlines for e_1=0.86, Fr=5, α=0° and respectively Gr=10^2, Gr=10^3, Gr=10^4 and Gr=5.10^4

We can say that the heat transfer is mainly conductive. The values of the streamline which are given on the corresponding figure are very small.

For Gr=10^3 the isothermal lines are transformed symmetrically with respect to the vertical axis and change significantly, and the values of the streamlines mentioned on the same figure, increase also significantly, which translates a transformation of the conductive transfer to the convective transfer, but relatively low as shown in the isotherms shape.

However for Gr=10^4 the isotherms are modified and eventually take the form of a mushroom. The temperature distribution decreases from the hot wall to the cold wall. The direction of the deformation of the isotherms is consistent with the direction of rotation of the streamlines. In laminar flow, we can say that under the action of the particles movement taking off from the hot wall at the symmetry axis, the isotherms move away from the wall there. The values of the stream functions increase which means that the convection intensifies.

The increase of the Grashof number to 5.10^4 intensifies the convection as shown in corresponding figures.
Let us note that the isotherms, of all the figures indicated above, were plotted with a ΔT^+=0.1

3.5 Local Nusselt Number

We determine the local Nusselt numbers for which changes along the walls are closely related to the distributions of isotherms and streamlines, so that, qualitatively, these variations and distributions can often be deduced from each other. For example, if we consider a current point on a wall following a coordinated observation of a monotonous reduction in the local Nusselt number corresponds to a directed flow following this coordinate, the observation of an increase corresponds to a directed flow in opposite direction.

3.6 Analogy between the variation of local Nusselt number -isotherms and streamlines

We thus notice on Figure 6, that the variations of local Nusselt number on the inner activate wall are in accordance

with what has just been indicated above, a minimum reflects an existence of two counter-rotating cells pushing away the fluid from the wall, a maximum reflected, on the contrary, the existence of two counter-rotating cells providing the fluid to the wall. What thus enables us to follow the evolution of our flow in our annular space.

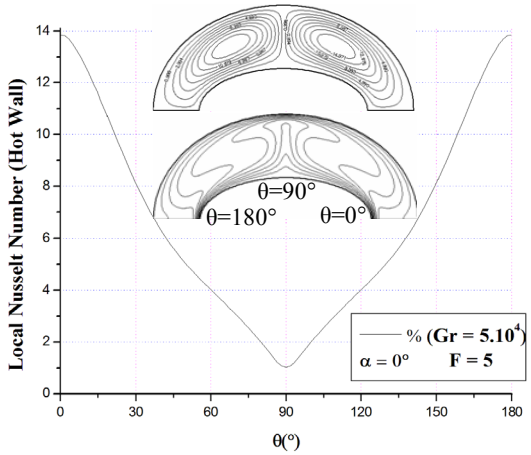

FIG. 6 Variation of local Nusselt number on the inner activate wall

3.7 Variation of local Nusselt number on the hot wall

Figure 7 illustrates the variation of local Nusselt number on the hot wall, and allows us to notice that with the increase of the Grashof number, the value of local Nusselt number on this wall also increases, which is obvious.

3.8 Effect of the angle of inclination α :

We examine here the effect of the inclination of the system compared to the horizontal plane, the angle α is measured from the horizontal plane in the trigonometric direction. We used two values of α (0° and 45°).

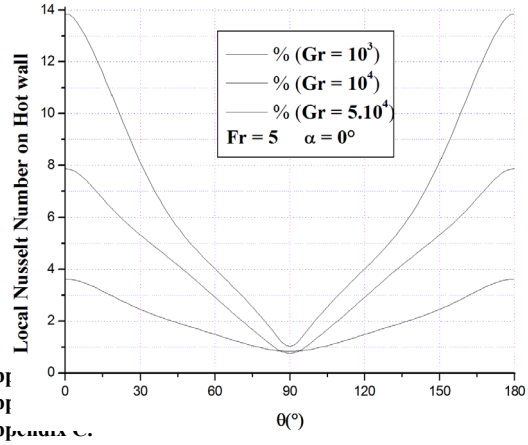

Appendix C.

FIG. 7 Variation of local Nusselt number on the hot wall

Appendix D.

3.9 Case where the inclination angle α is zero

In this case, the vertical fictitious median plane is in principle a symmetry plane for transfer phenomena. Therefore by symmetry and in relation to this vertical plane depending on the value of Grashof number, the flow is organized always in two principal cells rotating in opposite directions, as the figures (4-5) show.

3.10 Case where the inclination angle α = 45°

When α=45°, the symmetry of the system relative to the fictitious vertical plane is destroyed as well illustrated in figure 8 and figure 9, the ends of annular space move upwards for the right part of the system and downwards for the left part. Figure 9 show that the cell of left can more develop that its counterpart on the right part and tends to occupy the entire annular space as the system is inclined more until becoming vertical.

3.11 Local and average Nusselt number

The figure 10 which illustrates the variation of local Nusselt number on the hot wall shows that for α=0° the minimum of local Nusselt number is reached at the angular position θ=90°, which is in agreement with figure 5 which shows that the two cells meet at this precise place while moving away the fluid from this wall. For α=45° the minimum of local Nusselt number moves at the position θ=53°, which is in agreement also with figure 9 which shows that for this inclination, the two cells meet at this angular position while moving away the fluid there from this wall.

FIG. 8 Isotherms for e_1=0.86, Fr=5, α=45° and Gr=5.10^4

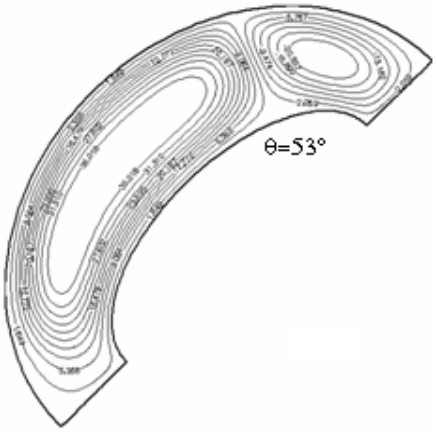

FIG. 9 Streamlines for e_1=0.86, Fr=5, α=45° and Gr=5.10^4

The variation of average Nusselt number on the hot wall as a function of Grashof number illustrated in figure 11 which shows that the inclination α is then without influence when Gr≤10^3, this translates that the heat transfer is primarily conductive. For the greatest values of the Grashof number, α influences the convective transfer.

CONCLUSION

We established a mathematical model representing the transfer of movement within the fluid and heat through the active walls of the enclosure. This model based on the assumption of Boussinesq and the bidimensionnality of the flow. We have developed a calculation code, based on the finite volume method, which determines the thermal and dynamic fields in the fluid and the dimensionless numbers of local and average Nusselt on the active walls of the enclosure, depending to the quantities characterizing the state of the system. The influence of the Grashof number and the inclination of the system, on the flow in stationary mode has been particularly examined.

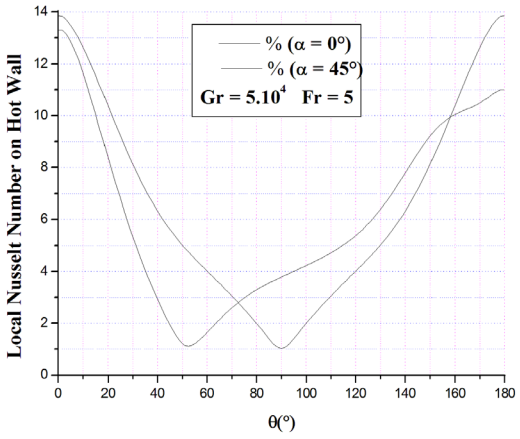

FIG. 10 Variation of local Nusselt number on the hot wall

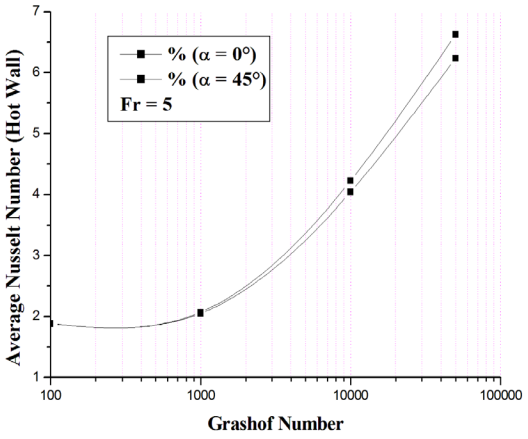

FIG. 11 Variation of the average Nusselt number on the inner activate wall

Appendix E.
Appendix F.
Appendix G.
Appendix H.
Appendix I.
Appendix J.
Appendix K.
Appendix L.
Appendix M.
Appendix N.
Appendix O.
Appendix P.
Appendix Q.

The results of the numerical simulations have shown that conduction is the regime of heat transfer dominant for Grashof numbers lower than 10^3. For Grashof numbers higher than 10^3, the role of the convection becomes dominant, this on the one hand, on the other hand we saw that the transfers are better when our system presents elements of symmetry.
Appendix R.

REFERENCES

[1] T.H.Kuehn, R.J. Goldstein, An experimental and theoretical study of natural convection in the annulus between horizontal cylinders, J. Fluid Mech., 74, 695-719, 1976.

[2] Y.D.Zhu, C. Shu, J. Qiu, J. Tani,Numerical Simulation of natural convection between two elliptical cylinders using DQ method, Int. J. Heat. Mass. Trans., 47, 797-808, 2004.

[3] M.Djezzar,M. Daguenet, Numerical study of bidimensional steady natural convection in a space annulus between two elliptic confocal ducts. 1ST International Conference on Thermal Engineering Theory and Applications. Beïrut-Lebanon, du 31 Mai au 04 Juin, 2004.

[4] M.Djezzar,M. Daguenet, Contribution to the study of the convection in various annular spaces, subjected to various conditions of heating. Thesis of Doctorate of state, University Mentouri Constantine, 2005.

[5] M.Djezzar,A. Chaker,M. Daguenet, Numerical study of bidimensional steady natural convection in a space annulus between two elliptic confocal ducts: Influence

of internal eccentricity. Revue des Energies Renouvelables. 8, 63-72, 2005.

[6] M.Djezzar,M. Daguenet, Natural steady convection in a space annulus between two elliptic confocal ducts: Influence of the slope angle. Journal of Applied Mechanics Transaction of the ASME, 72, 88-95, 2006.

[7] S.V.patankar , Numerical Heat Transfer and fluid flow, (McGraw-Hill book company), ppc113-137. New York,1980.

[8] P.Moon, E. Spencer, Field theory Engineers, (D. VAN. Nostrand company), p 356. LTD, Torronto,, Canada , 1961.

[9] E.F.Nogotov, Applications of Numerical Heat Transfer, (McGraw-Hill book company), ppc122-125. New York, 1978.